



# A Moth–Flame Optimization for UPFC–RFB-Based Load Frequency Stabilization of a Realistic Power System with Various Nonlinearities

Mahendra Nandi<sup>1</sup> · Chandan Kumar Shiva<sup>2</sup> · Vivekananda Mukherjee<sup>3</sup>

Received: 25 May 2016 / Accepted: 22 October 2018 / Published online: 3 November 2018  
© Shiraz University 2018

## Abstract

In this article, a realistic multi-area multi-source test power system model is investigated by imposing the effects of nonlinearities for the betterment of automatic generation control (AGC) realization. The confined area of presented work is to cogitate the effectiveness of combined unified power flow controller (UPFC) and redox flow battery (RFB) in view of damping of oscillations subjected to increased load perturbation. The investigated power system model is a six-area system having reheat thermal, hydro and gas-generating units lumped together in each control area. The present prospect analyzes a very realistic approach of AGC by adding physical constraints like time delay, governor dead band, boiler dynamics, reheat turbine and generation rate constraint to the aforesaid system. A nature-inspired novel moth–flame optimization (MFO) algorithm is employed as an optimization tool in the design of proportional–integral–derivative gains and the tunable parameters of UPFC and RFBs. The substantial point of discussion is the guaranteed convergence mobility as the moths in this algorithm update their positions with respect to the flames which represent the most promising solutions. The MFO-based results are compared with genetic algorithm-based method to show the superiority of MFO over other similar metaheuristic optimization techniques. Robustness of the designed controller is also studied over  $\pm 25\%$  uncertainties in parametric values and under loaded condition. The simulation works showed that the inclusion of UPFC and RFB is very much effective in load frequency stabilization and is quite robust for a realistic power system.

**Keywords** Load frequency stabilization · Moth–flame optimization · Realistic test model · Redox flow battery · Unified power flow controller

## List of symbols

$ACE_i$  Area control error of the  $i$ th area  
 $b_g$  Gas turbine constant of valve position (s)  
 $B_i$  Frequency bias constant of the  $i$ th area (p.u.MW/Hz)

$c_g$  Gas turbine valve position  
 $D$  System damping (p.u.MW/Hz)  
 $f$  Nominal system frequency (Hz)  
 $H$  Inertia constant (s)  
 $i$  Subscript, referred as the  $i$ th area  
 $K_{pi}$  Power system gain constant of the  $i$ th area (Hz/p.u.MW)  
 $K_p, K_i, K_d$  Proportional, integral and derivatives gains, respectively  
 $K_{rfb1}, K_{rfb2}$  Gains of RFBs  
 $K_{ri}$  Reheat gain constant of the  $i$ th area  
 $K_{upfc}$  Gain of UPFC  
 $N$  Filter coefficient  
 $P_{rt}$  Rated capacity of the area (MW)  
 $R_g, R_h, R_t$  Speed regulation parameters of gas, hydro and thermal units, respectively (Hz/p.u.MW)  
 $T_{cd}$  Gas turbine compressor discharge volume time constant (s)  
 $T_{cr}$  Gas turbine combustion reaction time delay (s)

✉ Vivekananda Mukherjee  
vivek\_agamani@yahoo.com

Mahendra Nandi  
nandimahendra72@gmail.com

Chandan Kumar Shiva  
dr.ck\_shiva@srecwarangal.ac.in

<sup>1</sup> Department of Electrical Engineering, Asansol Engineering College, Asansol, India

<sup>2</sup> Department of Electrical and Electronics Engineering, S R Engineering College, Ananthasagar, Hasanparthy, Warangal, Telangana, India

<sup>3</sup> Department of Electrical Engineering, Indian Institute of Technology (Indian School of Mines), Dhanbad, Jharkhand, India

$T_d$	Time delay (s)
$T_f$	Gas turbine fuel time constant (s)
$T_{gi}$	Governor time constant of steam turbine of the $i$ th area (s)
$T_{ij}$	Synchronizing coefficient
$T_{pi}$	Power system time constant of the $i$ th area (s)
$T_{rfb1}, T_{rfb2}$	Time constant of RFBs (s)
$T_{rh}$	Hydro turbine speed governor transient droop time constant (s)
$T_{ri}$	Reheat time constant (s)
$T_{rs}$	Hydro turbine speed governor reset time (s)
$T_{sg}$	Hydro turbine speed governor time constant (s)
$T_{ti}$	Steam turbine time constant of the $i$ th area (s)
$T_{upfc}$	Time constant of UPFC
$T_w$	Starting time of water in penstock (s)
$T_{wb}$	Time constant of washout block
$T_1, T_3$	Lead time constant (s)
$T_2, T_4$	Lag time constant (s)
$V_r$	Receiving-end voltage
$V_s$	Sending-end voltage
$V_{se}$	Series voltage magnitude
$V_{sh}$	Shunt voltage magnitude
$V_{ser}$	Voltage magnitude of series converter
$V_{shr}$	Voltage magnitude of shunt converter
$X$	Reactance of transmission line
$Y_c$	Lag time constant of gas turbine speed governor (s)
$\delta$	Load angle
$\delta_{ser}$	Phase angle of series converter
$\delta_{shr}$	Phase angle of shunt converter
$\varphi_{se}$	Phase angle of series voltage
$\varphi_{sh}$	Phase angle of shunt voltage
$\Delta f_i$	Frequency deviation of the $i$ th area (Hz)
$\Delta P_{tieij}$	Tie-line power flow deviation (p.u.MW)

## 1 Introduction

### 1.1 General

Modern power industries are being interconnected due to various reasons of economy and reliability. Each control area is connected to other areas via transmission line (called as tie-line) forming a secured power system. Tie-lines are mainly used to exchange power among the neighborhood areas to maintain inter-area support under normal and, even, in abnormal conditions. In a large capacity power system, generation of power is normally preferred from thermal, hydro and gas power plants. As concerned to total power generation, thermal-generating units contribute a major portion, whereas a hydro power

plant has to be operated with various constraints like water availability and speed regulation parameters (Sahu et al. 2015) and, hence, its contribution is less as compared to thermal power plant. As reflected by a gas-generating unit, it may respond to disturbances with quicker reaction time than steam turbine in sliding pressure mode, i.e., operation with steam control valves fully open (Saikia and Sahu 2013). It is ideally suitable for varying load demand and is normally used to meet the peak demand.

A power system is subjected to local variations in random load. The confined point is area load interruptions or any other undesirable system operations that cause deviations in system frequency and tie-line power from their nominal values. The solution made for this problem is known as load frequency control (LFC). On the other hand, automatic generation control (AGC) provides an additional control action that in conjugative works with governor system to die-out frequency deviation and even tie-line power oscillations after sudden load perturbations (Bevrani 2009). Throughout the operating condition, frequency is a common factor and a change in active power demand at one point is reflected at some other point of the system (Bevrani 2009; Arya 2018).

### 1.2 Literature Review

Practically, a control area may have more than one generating units which is connected to other areas of similar nature or of different ones. Integrating different nature of generating units to a common grid and its LFC performance study, subjected to load perturbation, has always been a difficult task for the researchers. At the same time, it is presumed to be an interesting subject of concern. In view of this, design of multi-generating units-based power system having active participation of reheat turbine, hydro and gas power plants owing to AGC mechanism has been studied in Parmar et al. (2012). The contributions of reheat turbine, hydro and gas power plants have been extended (Shiva and Mukherjee 2016) to deregulated AGC mode of operation having interconnected five-area power system.

A power system has many limitations and uncertainties while designing the equivalent model. The same has been observed in operating condition. To show these effects, physical constraints are imposed in the power system dynamics. By considering physical constraints, effects on frequency and tie-line power deviation quantity subjected to load change have been observed in Chandrakala and Balamurugan (2016). Literature survey reveals that some significant contributions have been achieved to minimize the effects of nonlinearity of power system while applying metaheuristic optimization techniques. In this context, a number of optimization techniques such as genetic algorithm (GA) (Golpira et al. 2011), gray wolf optimization

(Guha et al. 2016), hybrid firefly algorithm with pattern search technique (Sahu et al. 2015), bacterial foraging optimization (Saikia et al. 2011), hybrid gravitational search with pattern search technique (Sahu et al. 2015), ant lion optimizer (Raju et al. 2016), backtracking search (Guha et al. 2018), differential evolution (Sahu et al. 2015) have been used in the literature for control and optimization of controllers' parameters to enhance power system performance with imposed physical constraints. It is to be mentioned here that a number of optimization techniques have already been used. It is due to some merits/demerits as found in the optimization techniques when used for some specific problems. Therefore, the continued work is to be carried out on the improved design of the optimization techniques for the better solution of the problem.

Due to the increased size and complexity of modern power system, risks of load changes and system oscillations increase. Under this circumstance, it is difficult to maintain the balance between generation and load continuously without appropriate control. So, some additional auxiliary devices are essential to cancel the effects of random load changes and maintain the frequency at the standard value. In this context, the present need is the use of flexible alternating current (AC) transmission systems (FACTS) devices that may play crucial roles to control the power flow in the interconnected power systems. The detailed description on the FACTS devices and their working mechanism as damping controller owing to power system stability improvement has been elaborated in Panda et al. (2015).

The utilization of FACTS devices as AGC damping controller may be found in Mondal et al. (2014). In some extended works, several studies have been explored showing the potential of FACTS devices for better operation of interconnected power systems. AGC analysis with (a) thyristor controlled phase shifter (Praghnesha et al. 2012) (b) simultaneous impact of redox flow batteries (RFBs) and interline power flow controller (Chidambaram and Paramasivam 2013; Gorripotu et al. 2015) and (c) unified power flow controller (UPFC) and RFB (Sahu et al. 2015), confined in deregulated environment, has been presented in the literature. As regards interconnected power systems, an improved damping of oscillation with (a) RFB unit (Kouba et al. 2016), (b) thyristor controlled series compensator (Zare et al. 2015) and (c) UPFC and SMES (Pradhan et al. 2016) owing to AGC mechanism may also be noted from the literature.

Literature survey shows that both the application of optimization techniques and the utilization of FACTS devices may play vital roles in interconnected/restructured power system owing to LFC mechanism. With the imposed physical constraints and even with realistic power system models, some new optimization techniques may confer

better control action as occurred in the earlier works. The same goes for the utilization of some new FACTS devices for better damping of oscillations. Literature survey also reveals that coordination of FACTS devices supplemented with LFC control performs much better control action in place of an individual one.

### 1.3 Motivations Behind the Present Work

To have a more practical and realistic interconnected power system, a simplified approach is being adopted by adding some important physical constraints such as time delay ( $T_d$ ), governor dead band (GDB), boiler dynamics (BD) for thermal plants, reheat turbine and generation rate constraint (GRC) for taking maximum advantage of a realistic LFC study. Therefore, a very large integrated power system model having six areas is being investigated in this paper with the aforesaid uncertainties. In the studied test system, areas 4, 5 and 6 have been taken only to make the model complex and large and the purpose is to investigate LFC performance in such a model. The stated model may be assumed as a realistic one. This type of model has its own advantages and disadvantages. As concerned to advantages, reliability of the network topology is enhanced and more exchange of power through tie-line may be observed. Owing to the increased exchange of power through tie-lines, also because of environmental and economic reasons as well as deregulation, the AGC design strategy needs to be changed differently than the conventional one and that is the problem of concern in (Golpira et al. 2011). The main issue concerned with the complexity of system is that both the frequency and tie-line power deviation deviate from the rated values, simultaneously. Under such circumstances, it becomes quite difficult to maintain the system responses within scheduled limit. It is also confirmed that the physical constraints are imposed to test the model dynamics of the system more accurately. In response to this, AGC response increases overshoot and settling time and, hence, performance of the designed controller is degraded (Golpira et al. 2011). The important constraints that affect the power system dynamics are time delay, governor dead band and generation rate constraint (GRC).

Hydro power plant-generating units are normally adjusted as the response is faster to raise/lower the power. Thermal power plants have rate restrictions due to thermal stresses even though all units are expected to participate in primary frequency regulation. If additional RFB and UPFC are available, the system dynamic performance may further be improved. Thereby, in the present prospect, impacts of RFBs and UPFC devices to such an interconnected system are investigated in light of load frequency stabilization. The improvement in the system response is due to its quick

response upon the change in load variation. To compensate sudden load changes, a fast acting RFB unit is utilized in the feedback path. RFB is an active power source which is not only a fast energy compensating device for power consumption of large load but also acts as a frequency stabilizer (Chidambaram and Paramasivam 2013; Enomoto et al. 2002). The other prospect is the enhancement of power quality maintenance for decentralized power system (Sahu et al. 2015). In another control strategy, UPFC controller is connected in series with the tie-line to improve the damping of oscillation.

Literature survey clarifies that the performance of power systems depends on the controller structure and the involved techniques associated with the design of the controller. Hence, new controller and high-performance heuristic optimization algorithms are always of need for better handling of the real world problems. The designed controller must have the ability to eliminate any system output deviations and bring the system to its rated condition. For any metaheuristic algorithm, a good balance between exploitation and exploration should be maintained during search process to achieve good performance. In general, performance of any optimization technique depends on the proper selection of certain control parameters. For example, GA needs mutation rate and crossover rate (Debbarma et al. 2014), particle swarm optimization algorithm uses the inertia weight, social and cognitive parameters (Gozde et al. 2012; Pedersen and Chipperfield 2010) while differential evolution algorithm uses scaling factor and crossover rate (Sahu et al. 2015; Das et al. 2008). Proper selection of these control parameters affects the performance of the algorithm.

Moth–flame optimization (MFO) is a global optimizing method (Mirjalili 2015). It explores the search space and gives an optimal/near-optimal solution (Mirjalili 2015). It does not require any controlling parameter. Being inspired from this feature of MFO algorithm, it is proposed in the present work for the design of controller gains that may sustain the studied power system model subjected to local area load disturbances. It is expected that MFO algorithm is capable of solving the real world challenging problems with unknown and constrained search spaces (Mirjalili 2015). From (Mirjalili 2015), it may be presumed that this algorithm is very effective and presents competitive results as compared to other well-known nature-inspired algorithms.

#### 1.4 Contribution of this Article

The present article depicts a very realistic approach in designing a power system model incorporating all possible physical constraints and the same is studied in the AGC prospective. A new metaheuristic algorithm (like MFO) is

implemented for the design of adjustable gains of proportional–integral–derivative (PID) controller, UPFC unit and RFB device. In a confined way, the main contributions of the present work may be outlined as follows.

- A realistic test power system model (i.e., six-area interconnected test system) is studied imposing the effects of  $T_d$ , GDB, BD, reheat turbine and GRC nonlinearities.
- The effects of UPFC and RFBs are going to be established as oscillation damping for the load frequency stabilization problem.
- The reason for implementing the proposed MFO algorithm, as a perfect fit for the constrained optimization problem, is established.
- It attempts to explain why MFO is a better choice as compared to other similar metaheuristic optimization techniques (like GA) in the sense of providing global solution with respect to AGC study.
- It shows the reason why the proposed MFO–UPFC–RFB is a better damping controller than the studied controller like GA–UPFC–RFB for the AGC mechanism.
- Robustness of the proposed MFO–UPFC–RFB controller is justified.

#### 1.5 Layout of the Paper

The rest of the article is documented in the following sequences. The short descriptions on transfer function-based block diagram of PID, UPFC and RFB as damping controller and dynamics of the studied power system are stated in Sect. 2. Section 3 details the mathematical formulation of objective function, the involved physical constraints and the measure of performance indices for optimization task. A brief review on MFO algorithm is introduced in Sect. 4. Section 5 details the simulation-based results/observations of the present work. Finally, the resultant outcomes are concluded in Sect. 6.

## 2 Controller/System Investigated

### 2.1 PID Controller: Basic Structure

Several control strategies have been investigated so far to achieve improved performance of the interconnected power systems. It is easily understood that PID controller makes it more favorable to achieve zero ACE signal due to easy realization and its design methodology. Therefore, it is being used in this work in each area for the designed six-area power system model. The objective is to minimize each area error subjected to increased load demand.

Therefore, the total deviation in error, i.e., area control error (ACE) is confined as a single variable of interest that acts as a signal/input of the controller. The amount of area error of the  $i$ th area subjected to the  $j$ th area may be given by (1) (Bevrani 2009).

$$ACE_i = B_i \Delta f_i + \Delta P_{tie_{ij}} \tag{1}$$

In response to this, output signal ( $u_i$ ) may be given by (2)

$$u_i = K_{PID_i}(s) \times ACE_i \tag{2}$$

where the expression for  $K_{PID_i}(s)$  may be stated by (3) (Sahu et al. 2015; Gorripotu et al. 2015).

$$K_{PID_i}(s) = K_p + K_i \left( \frac{1}{s} \right) + K_d \left( \frac{sN}{s + N} \right) \tag{3}$$

The disturbance/noise may be created in the system due to the nonlinear control system, imposed physical constraints and unusual increase in load demand. Therefore, the structure of the implemented controller with first-order filter effect is shown in Fig. 1. The significance of the filter is to attenuate the high frequency noise as present in the input signal (Sahu et al. 2015).

For any fixed controller structure, there is always a trade-off between the conflicting objectives of load disturbance rejection (reducing frequency and tie-line power deviation to zero very quickly) and the amount of control effort required. In this case, the problem is inherently multi-objective and to have a fast suppression of load disturbance and a higher amount of controller effort is required.

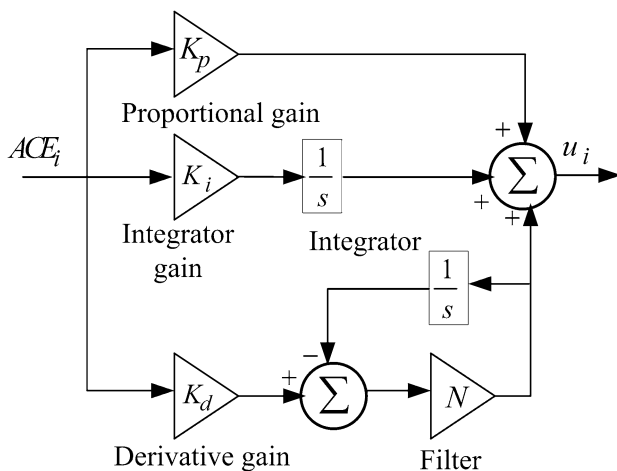


Fig. 1 Structure of the PID controller (Sahu et al. 2015; Gorripotu et al. 2015)

## 2.2 Linearized Model of UPFC

### 2.2.1 UPFC: Basic Concept/Configuration

UPFC is devised for the real-time control and dynamic compensation of AC transmission system. It provides multi-functional flexibility (Panda et al. 2015). It has the capability to control both the flow of real and reactive powers of transmission system by proper selection of firing angle of series and shunt converter (i.e.,  $\varphi_{se}$ ,  $\varphi_{sh}$ , in order) (Mondal et al. 2014). As per this ability, it is connected in series with the tie-line to improve the damping of oscillations. As the improvement in tie-line power is observed, the effect on frequency deviation, subjected to load perturbation, may be controlled. The reason for enhancing frequency stabilization in power system is to improve the system stability, alleviate system oscillations, enhance system controllability, increase power transfer capacity, mitigate sub-synchronous reactance and offer voltage stability (Mondal et al. 2014). Within the framework of traditional power transmission concept, UPFC is able to control, simultaneously or selectively, all the parameters affecting power flow in the transmission line (i.e., voltage, impedance and phase angle) (Panda et al. 2015). It is basically a combination of static synchronous compensator (STATCOM) and static synchronous series compensator (SSSC) connected via a common direct current (DC) link. STATCOM mainly controls the terminal voltage profile, whereas SSSC maintains the real power flow in the transmission line.

### 2.2.2 UPFC: Operating Scenario

UPFC simultaneously controls the real and the reactive power flow in a line. The active power required for the series converter is drawn by the shunt converter from the  $i$ th AC bus and supplies the  $j$ th bus via DC link. It may be noted here that the voltage magnitude of the output voltage provides voltage regulation while phase angle determines the mode of power flow control. The shunt converter may also generate reactive power in order to provide independent voltage regulation at its point of connection with the AC system (Mondal et al. 2014).

An equivalent circuit of UPFC is shown in Fig. 2 that consists of a shunt connected voltage source ( $V_{shr}$ ) and a series connected voltage source ( $V_{ser}$ ). The active power constraint equation links the two voltage sources. The two voltage sources are connected to the AC system through inductive reactance. The working range of UPFC angle is between  $-180^\circ$  and  $180^\circ$ . The expression of  $V_{shr}$  and  $V_{ser}$  is mathematically defined by (4)–(5) (refer Fig. 2), respectively (Mondal et al. 2014).

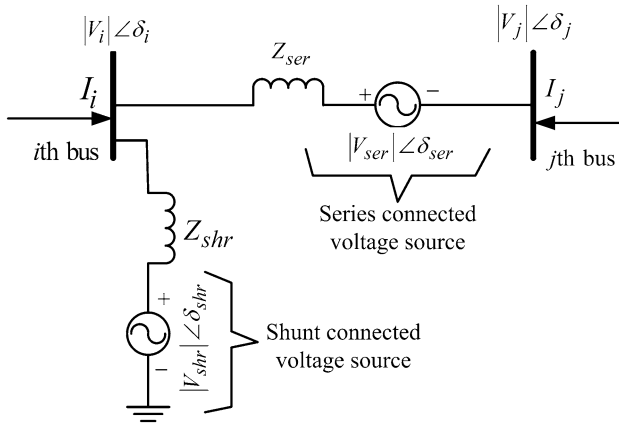


Fig. 2 Circuit diagram of UPFC stabilizer (Mondal et al. 2014)

$$V_{shr} = |V_{shr}|(\cos \delta_{shr} + j \sin \delta_{shr}) \tag{4}$$

$$V_{ser} = |V_{ser}|(\cos \delta_{ser} + j \sin \delta_{ser}) \tag{5}$$

The following observations may be made with the operating characteristics of UPFC (Mondal et al. 2014).

- a. If  $\delta_{ser}$  is in same phase with  $\delta_i$ , the real power flow between the  $i$ th and the  $j$ th bus is zero.
- b. If  $\delta_{ser}$  is in quadrature with  $\delta_i$ , the real power flow between the  $i$ th and the  $j$ th bus may be controlled via  $Z_{ser}$ .
- c. If  $0 \leq \delta_{ser} \leq 90^\circ$ , the real and the reactive power flow in the transmission line may be controlled.

From the viewpoint of conventional transmission control, a general power flow control capability of the UPFC may be best illustrated by a two-area power system model (refer Fig. 3) (Pradhan et al. 2016). As per this figure, a shunt converter injects controllable shunt voltage such that the real component of the current (in the shunt branch) balances the real power demanded by the series converter.

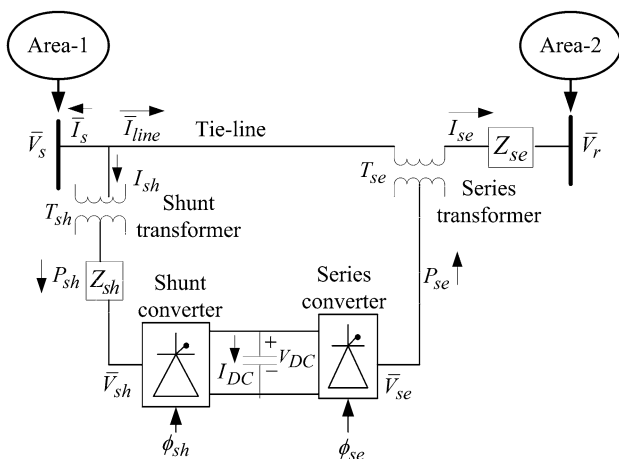


Fig. 3 Two-area interconnected power system with UPFC (Pradhan et al. 2016)

The tie-line power flow expression, neglecting the resistance of transmission line, is given by (6) (Panda et al. 2015)

$$P - jQ = V_r^* \left\{ \frac{V_s + V_{se} - V_r}{jX} \right\} \tag{6}$$

where  $V_{se} = |V_{se}| \sin(\delta - \phi_{se})$ .

After separating the real part, the expression for tie-line power flow may be expressed by (7).

$$P_{real} = \frac{V_s V_r}{X} \sin(\delta) + \frac{V_s V_{se}}{X} \sin(\delta - \phi_{se}) \tag{7}$$

In (7), if  $\delta$  is zero, the real power is uncompensated. As regards UPFC,  $V_{se}$  may be varied from 0 to  $V_{se}^{max}$ , whereas the phase angle may be changed between  $0^\circ$  and  $360^\circ$  (Verma et al. 2001). This wide range of control for the transmitted power indicates not only the superior capability of UPFC in power flow application but also suggests its powerful capability for transient stability improvement and power oscillation damping. This concept may be explored in regulating the tie-line power flow and, hence, to AGC mechanism.

### 2.2.3 UPFC: Utilization to AGC Mechanism

The structure of UPFC, as used for the purpose of load frequency stabilization, is shown in Fig. 4. The main components involved in UPFC stabilizer are (a) gain of UPFC, (b) washout block, (c) two-stage lag-lead compensator and (d) internal time delay of UPFC. A washout block serves as a high-pass filter that prevents the steady state changes in the speed with change in frequency (Mondal et al. 2014). In the present prospective, frequency deviation of area 1 ( $\Delta f_1$ ) is considered as input to the UPFC block. The transfer function representation of UPFC, as a frequency stabilizer, may be stated by (8).

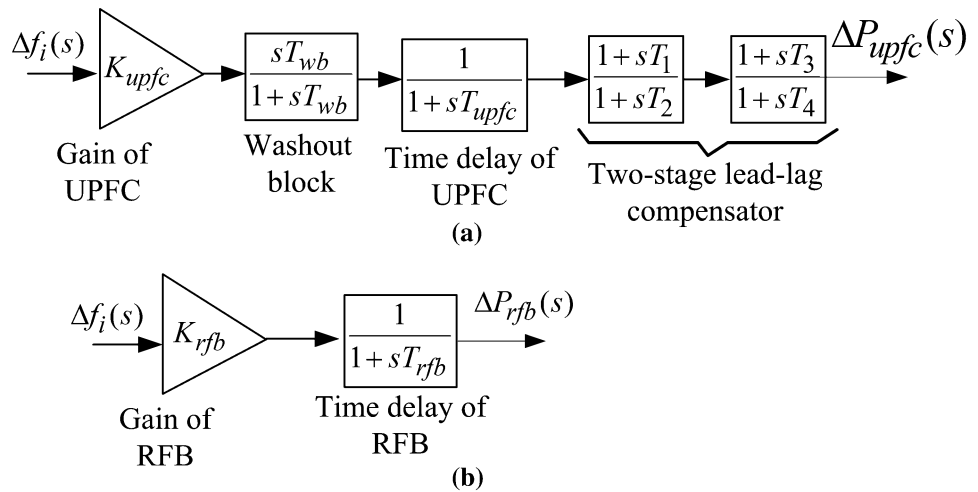
$$\frac{\Delta P_{upfc}}{\Delta f_1} = \left( \frac{K_{upfc}}{1 + sT_{upfc}} \right) \left( \frac{sT_{wb}}{1 + sT_{wb}} \right) \left( \frac{1 + sT_1}{1 + sT_2} \right) \left( \frac{1 + sT_3}{1 + sT_4} \right) \tag{8}$$

## 2.3 Linearized Model of RFB

### 2.3.1 RFB: Basic Concept/Configuration

RFB units are incorporated in the power system ensuring a very quick response upon the change in load variation. During very low load duration, the battery charges and delivers energy to the system when sudden load changes. Moreover, the phenomenon of hunting due to a delay in response does not occur and, therefore, improves the power quality (Chidambaram and Paramasivam 2013). In the context of RFB performance, (a) excellent short-time

**Fig. 4** Transfer function-based load frequency stabilizer: **a** UPFC (Mondal et al. 2014) and **b** RFB (Chidambaram and Paramasivam 2013; Gorripotu et al. 2015)



overload output response characteristics, (b) easy operation at normal temperature, (c) very small losses during operating conditions, (d) long service life and (e) effects on generation control and the absorption of power fluctuation needed for power quality maintenance are well established in Chidambaram and Paramasivam (2013), Enomoto et al. (2002). A general block diagram of the RFB, showing its working characteristic/nature, is shown in Fig. 5 (Gorripotu et al. 2015). The dynamics of the RFB, for small signal analysis, are represented in Chidambaram and Paramasivam (2013), Gorripotu et al. (2015).

Recently, RFBs have been investigated in LFC scheme in order to enhance the system frequency response under loaded conditions. During the low load periods the battery charges, in contrast, during the peak load demands or sudden load changes, the battery delivers the energy back to the system. The RFB consists of flow type cells, electrolyte tanks, pumps and piping. The electrolytic reactions take place in the cell, while each electrolyte tank stores a solution of the active material. Each pump circulates the electrolyte between the tank and the electrolytic cells. The battery reactions which are responsible to change the valence of the vanadium in both the positive and negative electrodes occur when an electric current has loaded to the cell. The valence change moves protons through the membrane, charging or discharging the battery according to the above mechanism where the reactions that occur in

the battery cell during charging and discharging may be modeled as in (9)–(10) (Kouba et al. 2016).

Positive electrode

$$V^{4+} \rightleftharpoons V^{4+} \text{ electrode} + e^- \tag{9}$$

Negative electrode

$$V^{3+} + e^- \rightleftharpoons V^{2+} \tag{10}$$

The LFC signal is used directly as the command value to control the output of RFB, while the mathematical model is given by (11)–(13) (Kouba et al. 2016).

$$\frac{dP_{dox1}}{dt} = \frac{1}{T_{di}} ((K_{RFB} U) - P_{dox2} - P_{dox1}) \tag{11}$$

$$\frac{dP_{dox2}}{dt} = \frac{1}{T_{ii}} ((K_{ri} P_{dox}) - P_{dox2}) \tag{12}$$

$$P_{dox} = P_{dox1} - SP_{dox} \tag{13}$$

### 2.4 RFB: Utilization to AGC Mechanism

In the designed power system model, RFBs are connected in the feedback loop. RFB absorb (or release) energy from or to the grid if there is a surplus (or deficit) in power. As RFB is capable of ensuring very quick response,  $\Delta f_i$  may be directly used as the input command signal. In the present work, two RFB units (one in area 1 and the other one in area 2) are used. For sudden step load perturbation (SLP), the change in outputs of RFBs ( $\Delta P_{rfb1}$ ,  $\Delta P_{rfb2}$ ) may be given by (14)–(15) (Chidambaram and Paramasivam 2013; Gorripotu et al. 2015).

$$\Delta P_{rfb1} = \frac{K_{rfb1}}{1 + sT_{rfb1}} \Delta f_1 \tag{14}$$

$$\Delta P_{rfb2} = \frac{K_{rfb2}}{1 + sT_{rfb2}} \Delta f_2 \tag{15}$$

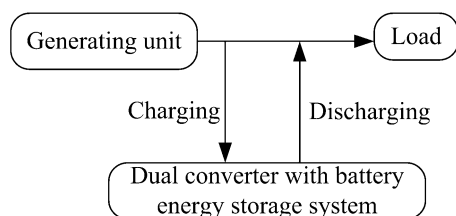


**Fig. 5** General block diagram of RFB for LFC (Sahu et al. 2015)

In (14),  $\Delta P_{\text{rfb1}}$  is the incremental control action taken by the centralized controller employed in the feedback to reduce the grid frequency oscillation (i.e.,  $\Delta f_1$ ). Similar implication goes for  $\Delta P_{\text{rfb2}}$ .

#### 2.4.1 Designed Test System: Interconnected Six-Area Power System

The investigated test system is a six-area system with each area consisting of reheat thermal, hydro and gas-generating units. Each area has identical capacity of 2000 MW with nominal loading of 1840 MW. To resemble a realistic approach, each area is equipped with physical constraints like  $T_d$ , GDB, BD, reheat turbine and GRC.

Any signal processing and data gathering introduce a time delay that should be properly considered in the AGC analysis. On the other hand, owing to the restructuring, expanding of physical setups, functionality and complexity of power systems in a new environment, communication delays become a significant challenge in the AGC analysis. In the view point of stability and performance analysis, it is shown that the impact of delay on the dynamic behavior of a control system is the same as the effect of perturbation and system uncertainty (Golpira et al. 2011). Similar to dynamic uncertainties, time delays can degrade system's performance and stability (Golpira et al. 2011). That is why it could be quite reasonable to consider the time delay as a model uncertainty (Bevrani 2009). Moreover, in this work, it is shown that the frequency control performance declines when the time delay increases. The BD configuration is incorporated in thermal plants to generate steam under pressure. This model considers the long-term dynamics of fuel and steam flow on boiler drum pressure as well as combustion controls (Sahu et al. 2015). Steam turbine GDB is defined as the change in speed subjected to no change in valve position. It is due to the backlash in the linkage connecting the servo piston to the camshaft. One effect of GDB is an increase/decrease in speed which may be observed before the position of the valve changes. It also has a great effect on the system dynamic performance of electric energy system (Sahu et al. 2015). In a power system, power generation can change only at a specified maximum rate known as GRC. The presence of GRC will adversely affect the system performance in LFC studies. Regarding these issues, an attempt is made to study the LFC issues in such a complex system considering important physical constraints, all together.

The configuration of the boiler dynamics, as used in the present model, is shown in Fig. 6 (Chandrakala and Balamurugan 2016). The relevant model parameters (such as system configuration, system parameters, participation factor, imposed physical constraints, boiler dynamics and

the gains of UPFC and RFB controllers) are appended in Sects. 7.1–7.4. It is assumed that all the generators are coherent in each area. In the designed model, the studied UPFC is placed nearer to area 1 which is connected in series with the tie-line whereas one RFB unit is connected to both the load points of area 1 and area 2. Figure 7 represents the simplified representation of the designed power system model, whereas its configuration of the  $i$ th area is depicted in Fig. 8. Each area of the designed power system model is equipped with a PID controller.

### 3 Problem Formulation

The objective of the present work is to minimize the amount of error of each area after a sudden load perturbation. The point of focus is to maintain the area frequency and the tie-line power oscillations to their respective nominal values within the shortest period of time. Therefore, for decentralized control mechanism in each area, an UPFC and two RFBs (as damping controllers) are added to the system dynamics for the betterment of the system performance. Here, the LFC problem is considered as constrained optimization problem and the MFO algorithm is proposed as an optimizing tool. The other points are to investigate the efficacy, the potential and the dominance of the proposed MFO algorithm over other similar population-based optimization techniques in LFC problem. Regarding problem formulation, three important mathematical terms such as objective function, constraints of the optimization mechanism and measure of performance appear in the next three subsections, in sequence.

#### 3.1 Objective Function

To minimize the fitness value for finding the optimized solution of load frequency stabilization problem, the figure of demerit (FOD) (considered here as an integral of time multiplied absolute error (ITAE)) is chosen as objective function for the present work. The expression for FOD may be stated by (16).

$$\text{FOD} = \text{ITAE} = \int_0^{t_s} (|\Delta f_i| + |\Delta P_{\text{tie},ij}|) t dt \quad (16)$$

In (Shabani et al. 2013; Abdel-Magid and Dawoud 1995), it has been revealed that integral of absolute error (IAE) and integral of square error (ISE) decrease the maximum overshoot more than ITAE. ITAE has the advantage of decreasing settling time more than IAE and ISE. That clearly demonstrates why ITAE is chosen as objective function in the present work.



**Fig. 6** Configuration of boiler dynamics (Chandrakala and Balamurugan 2016)

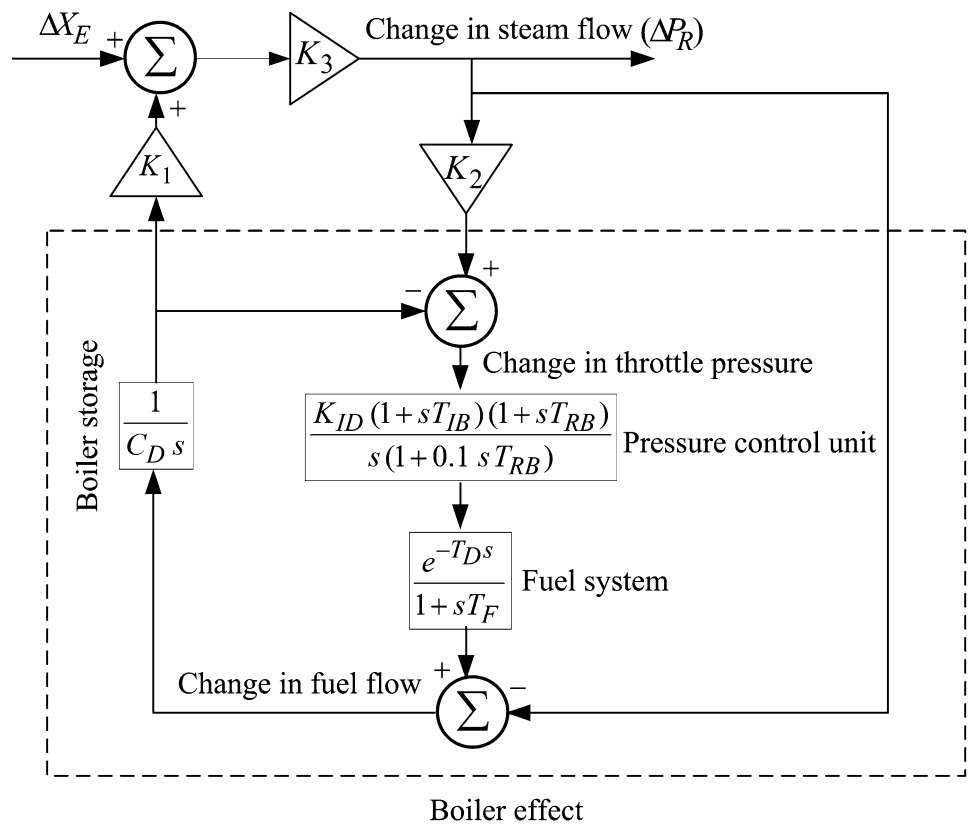
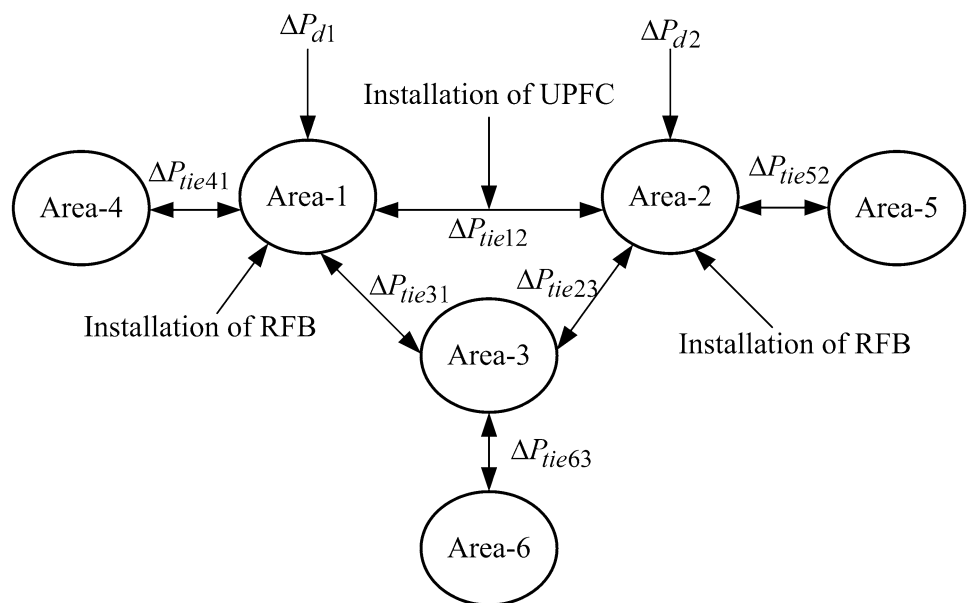


**Fig. 7** Simplified diagram of the designed six-area power system configuration



**3.2 Constrained Optimization**

The variables of interest chosen for a constrained optimization task are the gains of PID controller and the tunable parameters of UPFC and RFB. Therefore, the design problem may be considered as a constrained controller design problem. Thus, the present optimizing task is

defined in (17), while the limits of these optimizing variables may be framed by (18)–(20).

Minimize FOD (17)

subject to

- a. Constraints of PID parameters

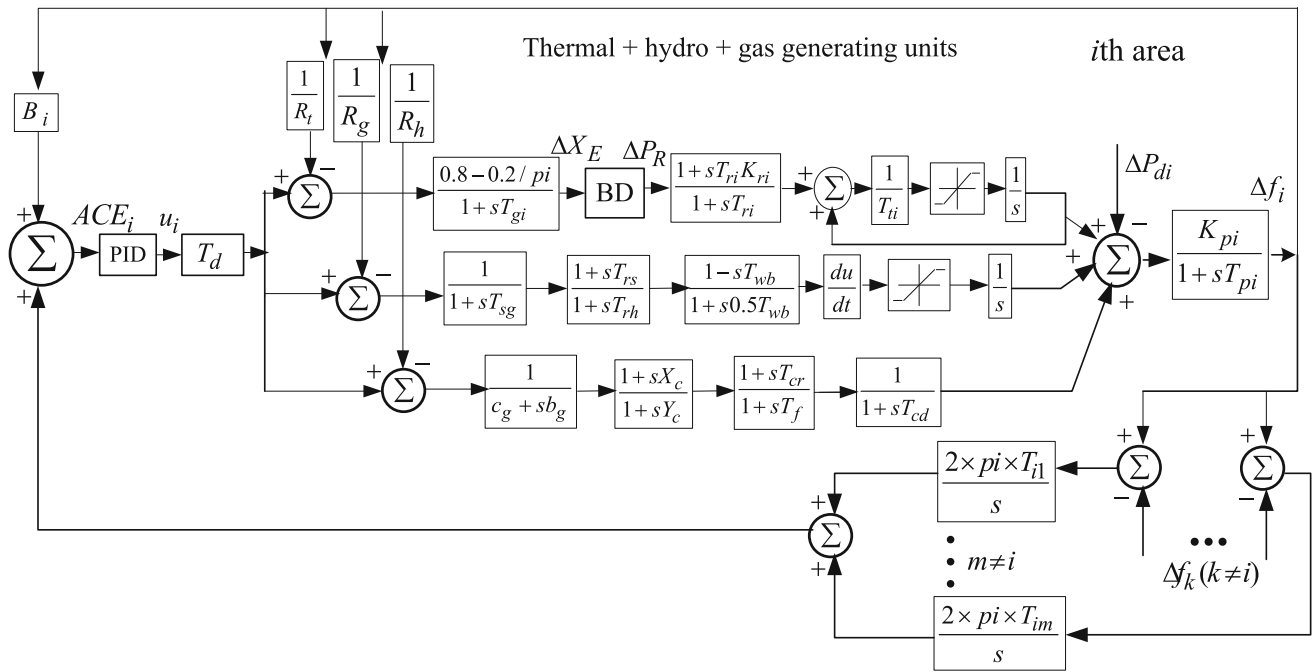


Fig. 8 Configuration of the *i*th area of the designed six-area power system model

$$\left. \begin{aligned}
 K_{pk}^{\min} \leq K_{pk} \leq K_{pk}^{\max}, \quad k = 1 - 6 \\
 K_{ik}^{\min} \leq K_{ik} \leq K_{ik}^{\max}, \quad k = 1 - 6 \\
 K_{dk}^{\min} \leq K_{dk} \leq K_{dk}^{\max}, \quad k = 1 - 6 \\
 N^{\min} \leq N \leq N^{\max}
 \end{aligned} \right\} \quad (18)$$

b. Constraints of UPFC parameters

$$\left. \begin{aligned}
 K_{upfc}^{\min} \leq K_{upfc} \leq K_{upfc}^{\max} \\
 T_{upfc}^{\min} \leq T_{upfc} \leq T_{upfc}^{\max} \\
 T_{wb}^{\min} \leq T_{wb} \leq T_{wb}^{\max} \\
 T_1^{\min} \leq T_1 \leq T_1^{\max} \\
 T_2^{\min} \leq T_2 \leq T_2^{\max} \\
 T_3^{\min} \leq T_3 \leq T_3^{\max} \\
 T_4^{\min} \leq T_4 \leq T_4^{\max}
 \end{aligned} \right\} \quad (19)$$

c. Constraints of RFB parameters

$$\left. \begin{aligned}
 K_{rfb1}^{\min} \leq K_{rfb1} \leq K_{rfb1}^{\max} \\
 T_{rfb1}^{\min} \leq T_{rfb1} \leq T_{rfb1}^{\max} \\
 K_{rfb2}^{\min} \leq K_{rfb2} \leq K_{rfb2}^{\max} \\
 T_{rfb2}^{\min} \leq T_{rfb2} \leq T_{rfb2}^{\max}
 \end{aligned} \right\} \quad (20)$$

In (18)–(20), the superscripts min and max represent the minimum and the maximum values of the respective variables. One more important factor that affects the optimal solution more or less is the range for unknowns. The range of unknowns depends on the type of applications,

i.e., the problem considered. For the very first execution of the program, a wider solution space has been taken and, after getting the solution, one may shorten the solution space nearer to the values obtained in the previous iteration. This is to be repeated until approximate solution is met. After confirmation of the solution space, the optimization task was repeated many times and the best final solution among them is chosen as the controller parameters.

In the present optimization task, the minimum and the maximum values of the PID gains of each PID controller are 0.001 and 5, respectively; the range of *N* is 0.001 to 300; the UPFC parameters are defined between [0.001, 1]; the range of *T<sub>wb</sub>* is 0.001 to 50; the range of two lead-lag compensating device and the parameters of RFBs are to be confined in [0.001, 1]. The choice in the present case indicates that the design value gives more importance to the fast suppression of the frequency and tie-line power deviation in comparison to the higher value of control signal.

### 3.3 Measure of Performance

#### 3.3.1 Calculation of Eigenvalues

The damping of oscillations, as produced by the investigated controller, is closely related to the eigenvalues ( $\zeta$ ). The overall system stability, the oscillatory behavior and the characteristics of a system may be well explained by the location of its position in the *s*-plane (Ogata 1995). It

compares the exponential decay frequency of the response profile to the natural frequency (Nise 2006).

### 3.3.2 Calculation of Performance Indices

To justify the designed controller being more enhanced and to show its performance consistency, three additional performance indices are chosen in the present work and these are (a) IAE, (b) integral of time square error (ITSE) and (c) ISE. These three performance indices may be stated by (21)–(23), in order.

$$\text{IAE} = \int_0^{t_s} (|\Delta f_i| + |\Delta P_{tie\ ij}|) dt \quad (21)$$

$$\text{ITSE} = \int_0^{t_s} \{(\Delta f_i)^2 + (\Delta P_{tie\ ij})^2\} t dt \quad (22)$$

$$\text{ISE} = \int_0^{t_s} \{(\Delta f_i)^2 + (\Delta P_{tie\ ij})^2\} dt \quad (23)$$

### 3.3.3 Transient Analysis: Parameter Evaluation

The objective of the current article is to characterize transient specifications associated with the obtained responses. A detailed description of the obtained responses is very necessary for the analysis and the design purposes. Therefore, the calculated transient parameters are rise time ( $T_r$ ), settling time ( $T_s$ ), peak value ( $M_p$ ) and peak time ( $T_p$ ). These parameters give information about the speed or nature of the transient responses (Nise 2006). The eigenvalues, the values of the studied three performance indices (such as IAE, ITSE and ISE) and the transient parameters are calculated at the end of the developed program.

## 4 MFO Algorithm

### 4.1 MFO: Basic Posture

MFO algorithm is based on the transverse orientation for navigation (Mirjalili 2015). In general, MFO algorithm uses the characteristics of moths. Analytically, the characteristic of moth is its special navigation at night and it maintains a fixed angle with respect to the moon (a very effective mechanism for traveling long distances in a straight line). The other point is the moth eventually moves toward the light. This behavior is, mathematically, used in the design of MFO algorithm for solving optimization problem (Mirjalili 2015).

### 4.2 MFO: Mathematical Posture

In terms of mathematical analogy, moths are analogous to the candidate solution and the positions of moths are analogous, in a confined search space, to the problem variables. It is assumed that the moths may travel in 1- $d$ , 2- $d$ , 3- $d$  or hyper-dimensional search space with change in their position vectors. Similar to population-based algorithm, the set of moths may be represented by (24) (Mirjalili 2015).

$$M = \begin{bmatrix} m_{1,1} & m_{1,2} & \cdots & \cdots & m_{1,d} \\ m_{2,1} & m_{2,2} & \cdots & \cdots & m_{2,d} \\ \cdot & \cdot & \cdot & \cdot & \cdot \\ \cdot & \cdot & \cdot & \cdot & \cdot \\ \cdot & \cdot & \cdot & \cdot & \cdot \\ m_{n,1} & m_{n,2} & \cdots & \cdots & m_{n,d} \end{bmatrix} \quad (24)$$

In (24),  $n$  is the number of moths whereas  $d$  is the dimension of the problem variables. For each moth, there is a corresponding fitness value. These may be given by (25) (Mirjalili 2015).

$$OM = [OM_1, OM_2, \dots, OM_n]^T \quad (25)$$

The MFO algorithm has a key component termed as flame which may be presented by (26) (Mirjalili 2015).

$$F = \begin{bmatrix} F_{1,1} & F_{1,2} & \cdots & F_{1,d} \\ F_{2,1} & F_{2,2} & \cdots & F_{2,d} \\ \cdot & \cdot & \cdot & \cdot \\ \cdot & \cdot & \cdot & \cdot \\ \cdot & \cdot & \cdot & \cdot \\ F_{n,1} & F_{n,2} & \cdots & F_{n,d} \end{bmatrix} \quad (26)$$

Similar to (24), each flame assumes its corresponding fitness value and may be given by (27) (Mirjalili 2015).

$$OF = [OF_1, OF_2, \dots, OF_n]^T \quad (27)$$

The MFO algorithm is based on three segments that estimate the global solution which may be stated by (28) (Mirjalili 2015).

$$\text{MFO} = (I, P, T) \quad (28)$$

In (28), the function  $I$  generates a random population of moths and the corresponding fitness values. The mathematical form of this function may be presented by (29) (Mirjalili 2015).

$$I: \phi \rightarrow \{M, OM\} \quad (29)$$

In (29), the function  $P$  defines the updated mechanism of moths in the search space. This function eventually returns the updated version of matrix  $M$ . This function may be presented by (30) (Mirjalili 2015).

$$P: M \rightarrow M \quad (30)$$

If the termination criterion is satisfied, the function  $T$  returns true, otherwise false. This may be stated in (31) (Mirjalili 2015).

$$T : M \rightarrow \{true, false\} \tag{31}$$

Based on (28)–(31), a general structure of the MFO algorithm is shown in Algorithm 1 (Mirjalili 2015).

The function  $I$  has to calculate the objective function values after generating the initial solutions. In this process, any random distribution is allowed. This is shown in Algorithm 2. In Algorithm 2, there are two arrays, called  $ub$  and  $lb$  (defining the upper and the lower bounds of the variables, respectively). These two may be presented in (32)–(33), in order.

---

**Algorithm 1:** General structure of the MFO algorithm [31]

---

```

M = I( );
while T(M) is equal to false
    M = P(M);
end
    
```

---

**Algorithm 2:** Calculation of the fitness function [31]

---

```

for i = 1 : n
    for j = 1 : d
        M(i, j) = (ub(i) - lb(i)) * rand( ) + lb(i);
    end
end
OM = FitnessFunction(M)
    
```

---

$$ub = [ub_1, ub_2, ub_3, \dots, ub_{n-1}, ub_n] \tag{32}$$

$$lb = [lb_1, lb_2, lb_3, \dots, lb_{n-1}, lb_n] \tag{33}$$

It may be noted here that both the moth and the flame are different from each other on the basis of update process (in its value) in each iteration cycle. The moths are real searching agents that roam around the search space(s), whereas the flames are the best position of moths during the optimization process. This may be analytically presented in (34) (Mirjalili 2015)

$$M_i = S(M_i, F_j) \tag{34}$$

where  $M_i$  indicates the  $i$ th moth,  $F_j$  indicates the  $j$ th flame and  $S$  is the spiral function.

A logarithmic spiral movement that dictates the updated position of moths around flames may be presented in (35) (Mirjalili 2015)

$$S(M_i, F_j) = D_i e^{bt} \cos(2\pi t) + F_j \tag{35}$$

where  $D_i$  is the distance of the  $i$ th moth for the  $j$ th flame,  $b$  is a constant that decides the shape of the logarithmic spiral, and  $t$  is a random number in  $[-1, 1]$ . The variable  $D$  may be calculated by (36).

$$D_i = |F_j - M_i| \tag{36}$$

In order to improve the probability of finding better solutions, the best solutions considered so far are the flames. During the process of optimization, moths have to update their positions with respect to the flames. In order to improve the quality of solution further, it is assumed that  $t$  is a random number in  $[r, 1]$  where  $r$  is linearly declined from  $-1$  to  $-2$  throughout the course of iteration. In this process, the moths tend to exploit their respective flames more accurately according to the number of iterations.

In the search space, the position updating process of moths may degrade the exploitation of the best solution with respect to the  $n$  different locations. To resolve this concern, an adaptive mechanism may be used for the number of flames. The number of flames, over the course of iteration, may be stated by (37)

$$\text{Flame\_number} = \text{round} \left( N_f - l \times \frac{N_f - 1}{T} \right) \tag{37}$$

where  $l$  represents the current number of iteration,  $N_f$  is the maximum number of flames, and  $T$  is the maximum number of iterations. The moths update their positions with respect to the best flame in the final step of iteration. The gradual decrement in number of flames balances the exploration and the exploitation of the search space.

In view of the above, the general steps of the function  $P$  are shown in Algorithm 3. The execution of the function  $P$  is continued until it returns the true value. After termination, the best moth is returned as the optimized solution. The flowchart of the proposed MFO algorithm compatible with the pseudo-code is presented in Fig. 9.

**Algorithm 3:** General steps for the update mechanism of moth [31]

Update flame number using (37)

$$OM = \text{FitnessFunction}(M)$$

**If** iteration == 1

$$F = \text{sort}(M);$$

$$OF = \text{sort}(OM);$$

**else**

$$F = \text{sort}(M_{t-1}, M_t);$$

$$OF = \text{sort}(M_{t-1}, M_t);$$

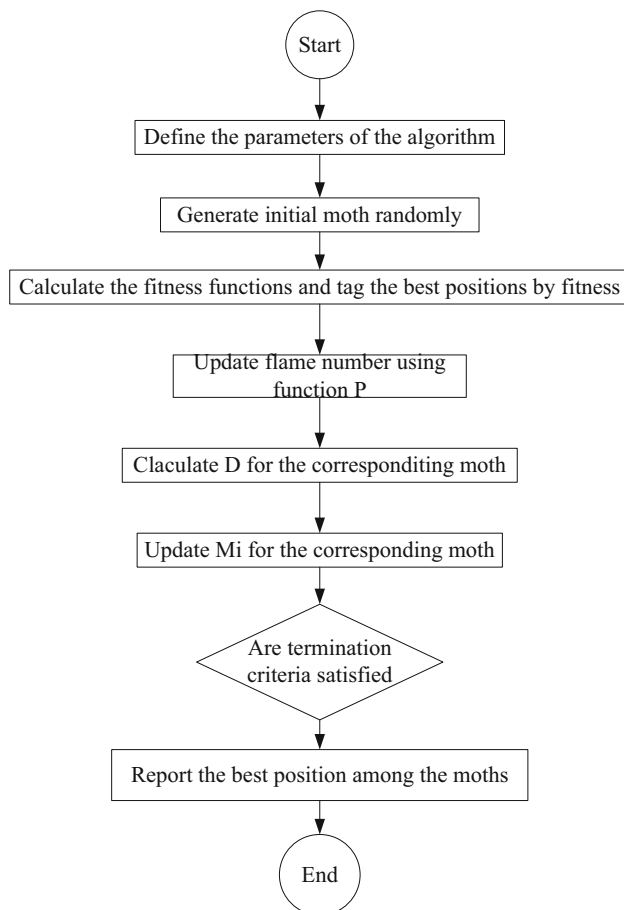
**end****for**  $i = 1:n$ **for**  $j = 1:d$ Update  $r$  and  $t$ Calculate  $D$  using (36) with respect to the corresponding mothUpdate  $M(i, j)$  using (34) and (35) with respect to the corresponding moth**end****end**

Fig. 9 Flowchart of the MFO algorithm

## 5 Simulation Results and Analysis

In the present study, the proposed MFO algorithm is applied to a six-area power system model equipped with UPFC and RFB units. In all the studied scenarios, the test system is investigated in presence of  $T_d$ , GDB, BD for thermal plants, reheat turbine and GRC. Simulations have been done only to show the ability of UPFC and RFB to support primary frequency control. Here, the issues concerning the integration of UPFC and RFB with the frequency regulation problem are discussed. The performance of the designed MFO–UPFC–RFB controller is compared with the studied GA–UPFC–RFB, employing the same ITAE objective function. During the result analysis, the contributions of UPFC (as damping controller) and the RFBs (as power supplement with quick response) in AGC prospective are going to be established for further improvement in system performance.

The applied load profiles for creating disturbances in the aforesaid system are shown in Fig. 10. The results of interest are bold faced in their respective tables. The major observations of the present work are documented below.

### 5.1 Scenario (a): SLP of 0.01 p.u. applied to area 1

In this scenario, an increased load demand of magnitude 0.01 p.u. is applied to area 1 of the investigated power system model. GA- and MFO-based optimized PID controller gains, corresponding to minimum objective function, are tabulated in Table 1. In response to this, the system dynamic performances are shown in Figs. 11 and

**Fig. 10** Studied load perturbation profiles: **a** SLP and **b** random SLP

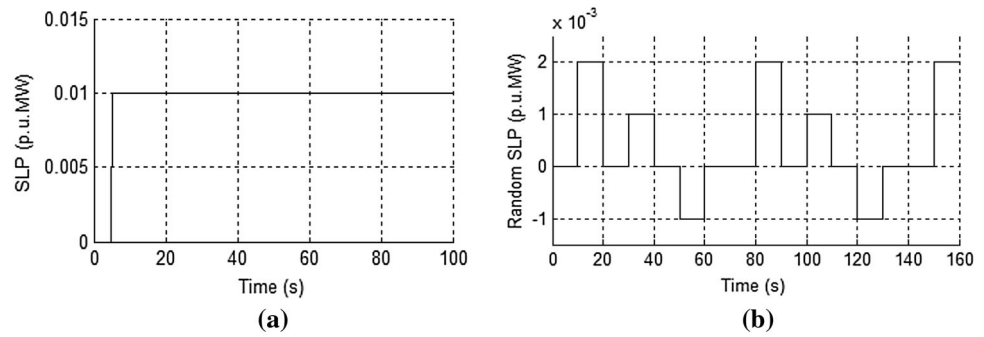


**Table 1** Optimized PID controller gains

Control area	GA-based [studied]			MFO-based [proposed]		
	$K_p$ (-ve)	$K_i$ (-ve)	$K_d$ (-ve)	$K_p$ (-ve)	$K_i$ (-ve)	$K_d$ (-ve)
Area 1	0.2195	0.3717	0.6293	2.9482	5.00	0.3844
Area 2	0.1454	0.1922	0.8166	2.0429	0.0010	3.1234
Area 3	0.2312	0.0361	0.7190	0.0043	0.0010	2.0895
Area 4	0.8790	0.8478	0.4693	1.1551	3.00	2.5485
Area 5	0.5434	0.4537	0.6254	0.9601	2.1682	1.8763
Area 6	0.9961	0.2781	0.6917	1.2471	1.3484	1.7133

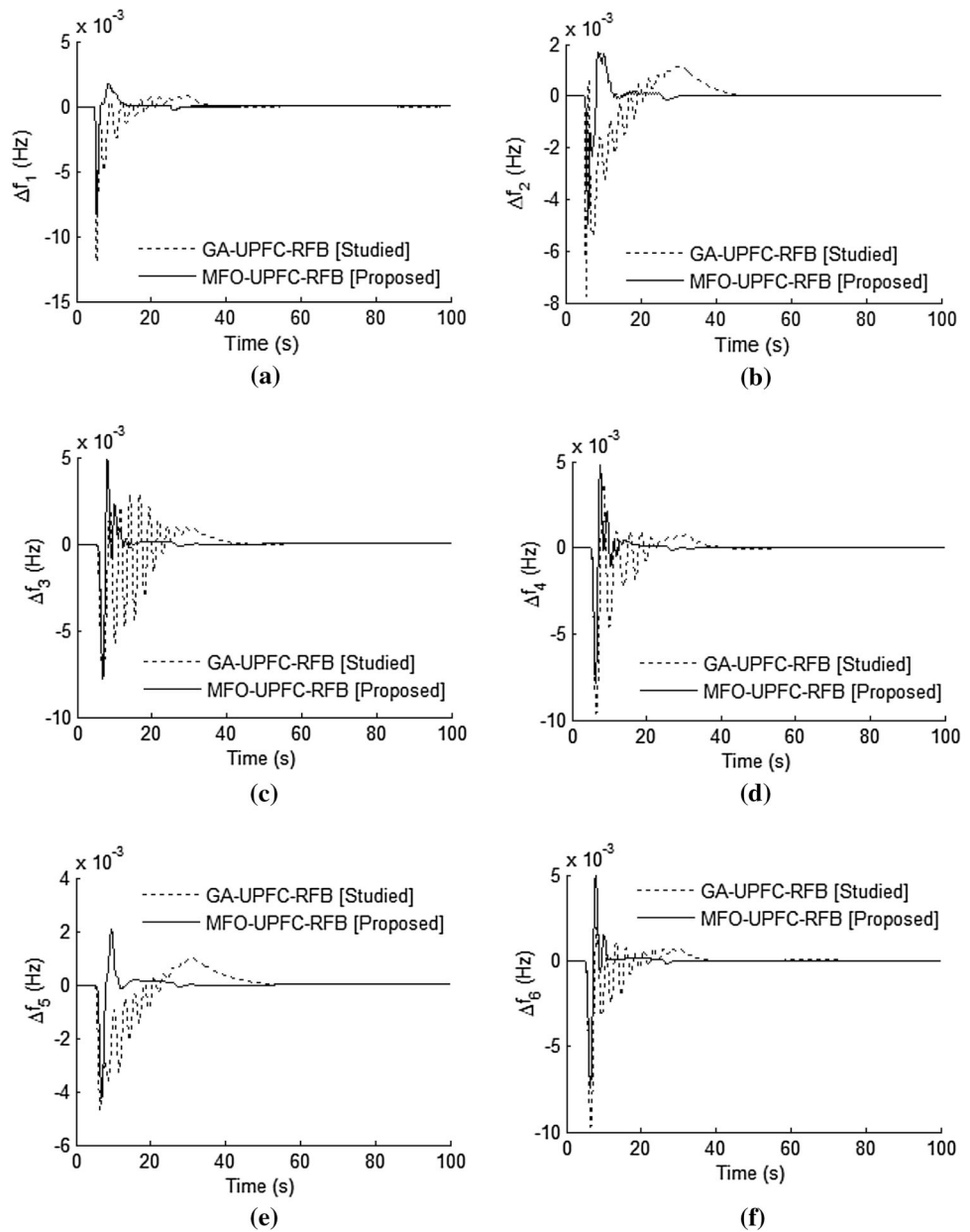
12. In Fig. 11, the response profiles of frequency deviations are presented in terms of  $\Delta f_1, \Delta f_2, \Delta f_3, \Delta f_4, \Delta f_5$  and  $\Delta f_6$ . The comparative study of convergence profile for the utilized optimization technique is shown in Fig. 12. The comparative tie-line power deviation profiles offered by the investigated damping controllers subjected to 0.01 p.u. SLP applied to area 1 in terms of  $\Delta P_{tie12}, \Delta P_{tie23}, \Delta P_{tie31}, \Delta P_{tie41}, \Delta P_{tie52}$  and  $\Delta P_{tie63}$  are shown in Fig. 13. For better comparison, the dynamic performances, as obtained with GA, are also shown in Figs. 11, 12, 13. All the presented response plots show that the control action, called for by the proposed MFO–UPFC–RFB controller, is better in comparison to the studied GA–UPFC–RFB one. It is clearly viewed from Figs. 11, 12, 13 that the proposed MFO has better dynamic stability in terms of settling time, overshoot and undershoot as compared to GA counterpart. Therefore, the governor action acts in a much better way for the proposed MFO algorithm.

The comparative values of eigenvalues for both the investigated methods are shown in Table 2. It shows that the proposed MFO–UPFC–RFB-based eigenvalues are away from the imaginary axis (of  $s$ -plane) as compared to GA–UPFC–RFB counterpart. This ensures better damping characteristics, and hence, the proposed MFO-based design controller is better than the GA one.

The comparative FOD and the studied performance indices (for the MFO- and the GA-based one) are presented in Table 3. Table 3 shows that the proposed MFO–UPFC–RFB controller offers lower FOD value as compared to the studied GA–UPFC–RFB one. These values are found to be **1.1706** and **7.1496**, respectively. Additionally, the values of three other performance indices (such as IAE, ITSE and ISE) also signify that the proposed MFO–UPFC–RFB controller is quite robust. The transient details, as offered by different investigated damping controllers subjected to 0.01 p.u. SLP applying to area 1, are tabulated in Table 4. It justifies the proposed MFO–UPFC–RFB controller generating better damping as compared to GA–UPFC–RFB counterpart (also see the Table 5). The system performance subjected to various operating conditions are also shown in Table 5. From this table, the same results may be obtained that MFO–UPFC–RFB controller is a better dynamic controller for the load frequency stabilization.

The comparative convergence profile of FOD value is also shown for both the investigated optimization techniques with ITAE-based objective function after application of 1% SLP in area 1 (refer Fig. 12). It may be observed that the proposed MFO algorithm shows better promising convergence characteristics as compared to GA counterpart. Minimization of MFO-based ITAE value, as

**Fig. 11** Comparative frequency deviation profiles offered by investigated damping controllers subjected to 0.01 p.u. SLP applied to area 1: **a**  $\Delta f_1$ , **b**  $\Delta f_2$ , **c**  $\Delta f_3$ , **d**  $\Delta f_4$ , **e**  $\Delta f_5$  and **f**  $\Delta f_6$



compared to GA-based one, shows that the proposed MFO is a better algorithm. This again shows that the optimized controller gains are better tuned in case of MFO as compared to GA. It may be noted that the optimization problem (in this case as load frequency optimization problem) has reached the near global optimal solution in case of MFO.

## 5.2 Scenario (b): Random SLP applied to area 1

To investigate the effectiveness of proposed controller, a different type of random load disturbances is applied to area 1. Figure 10(b) shows the random step load pattern as applied in this scenario. The step load is random both in magnitude and in duration. The variation in dynamic

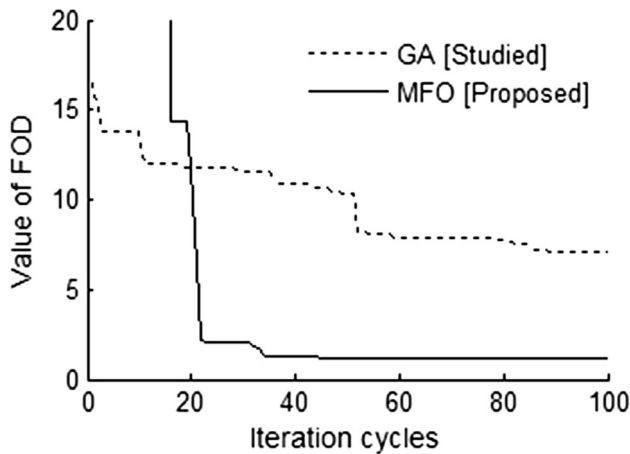
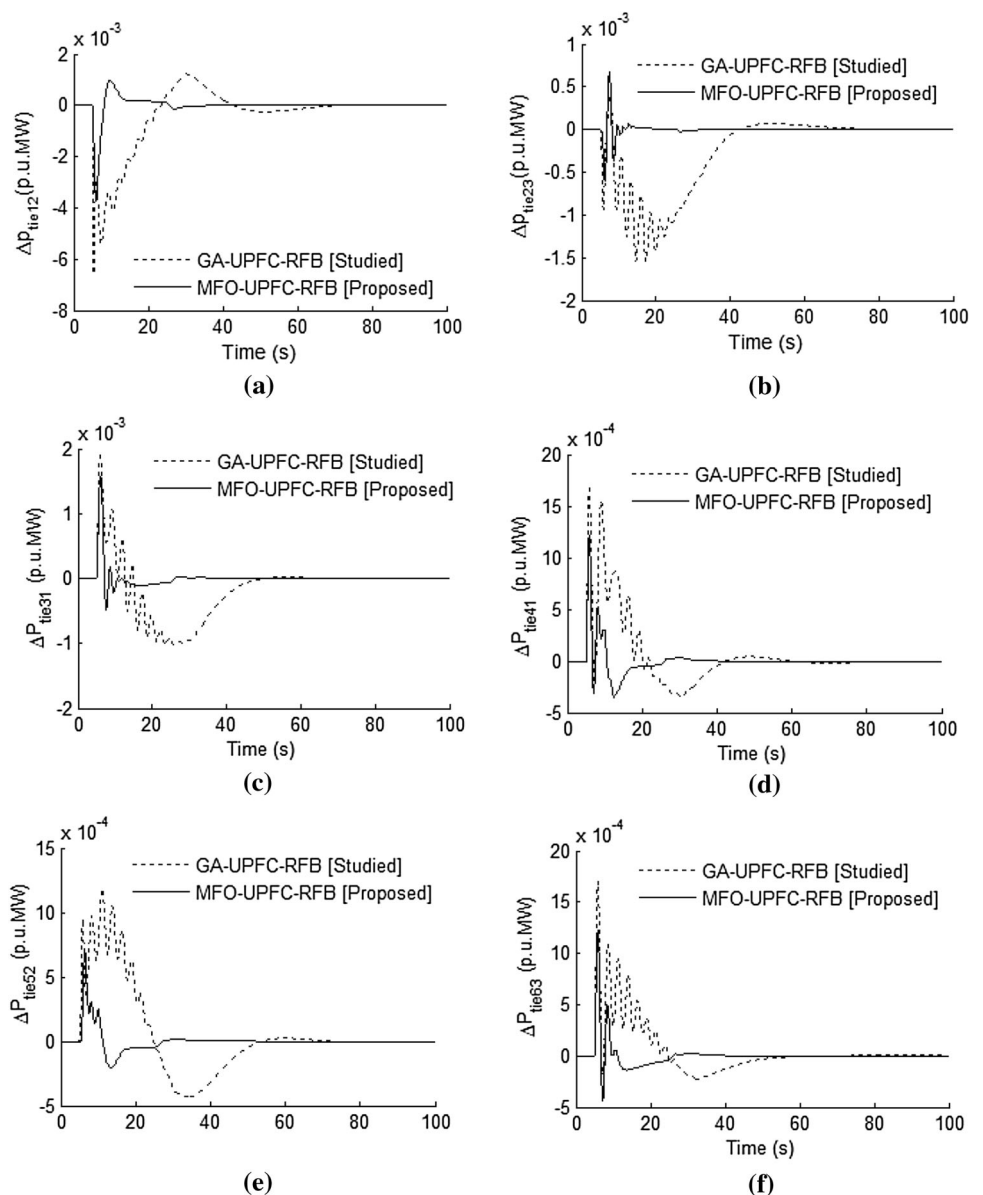


**Fig. 12** Comparative study of convergence profile for the utilized optimization technique

**Fig. 13** Comparative tie-line power deviation profiles offered by the investigated damping controllers subjected to 0.01 p.u. SLP applied to area 1: **a**  $\Delta P_{tie12}$ , **b**  $\Delta P_{tie23}$ , **c**  $\Delta P_{tie31}$ , **d**  $\Delta P_{tie41}$ , **e**  $\Delta P_{tie52}$  and **f**  $\Delta P_{tie63}$



response plots is shown in Figs. 14, 15. In Fig. 14, the response profiles of frequency deviations are presented and these are found to be the same as of scenario (a). The comparative tie-line power deviation profiles offered by the investigated damping controllers subjected to random load applied to area 1 are shown in Fig. 14.

From Figs. 14, 15, it is evident that the proposed MFO-based approach shows better transient responses when the system is incorporated with UPFC and RFB. The frequency deviation profile of area 1 shows that the proposed MFO-based design controller reaches its steady state value after each load perturbation. The same goes to the other stated response profiles also. The comparative dynamic response profile of error signals of area 1 and area 2 offered by investigated damping controllers in terms of  $ACE_1$  and  $ACE_2$  is shown in Fig. 16. Analysis shows that the



**Table 2** Comparative eigenvalues for the designed six-area GA-UPFC-RFB and MFO-UPFC-RFB-based power system models

GA-UPFC-RFB [studied]	MFO-UPFC-RFB [proposed]
	1.0e+003*
- 1.8182	- 0.0018
- 0.0348	- 0.0050
- 5.0000	- 0.0018
- 1.8182	- 0.0000
- 0.0348	- 0.0050
- 5.0000	- 0.0018
- 1.8182	- 0.0000
- 0.0348	- 0.0050
- 5.0000	- 0.0018
- 1.8182	- 0.0000
- 0.0348	- 0.0050
- 5.0000	- 0.0018
- 1.8182	- 0.0000
- 0.0348	- 0.0050
- 5.0000	- 0.0018
- 1.8182	- 0.0000
- 0.0348	- 0.0050
- 5.0000	- 0.0018
- 1.8182	- 0.0000
- 0.0348	- 0.0050
- 5.0000	- 0.9941
- 90.1154	- 1.0000
- 89.1892	- 0.3006
- 89.8417	- 0.3046
- 89.4853	- 0.3038
- 89.6505	- 0.3026
- 89.6109	- 0.3028
- 30.0100 ± 9.2449i	- 0.3031
- 6.9307 ± 12.1656i	- 0.0159
- 20.8960	- 0.0205
- 14.9351	- 0.0206
- 20.5372	- 0.0206
- 20.5205	- 0.0206
- 20.5284	- 0.0206
- 20.4964	- 0.0206
- 20.5278	- 0.0138
- 14.4881	- 0.0040 ± 0.0104i
- 14.7583	- 0.0120
- 15.3976	- 0.0114
- 14.6894	- 0.0110
- 3.0971 ± 6.5274i	- 0.0098
- 1.5070 ± 2.5449i	- 0.0052 ± 0.0052i
- 5.2899	- 0.0081
- 4.3285 ± 1.1364i	- 0.0045 ± 0.0043i
- 4.2422 ± 1.0834i	- 0.0049 ± 0.0038i
- 4.1613 ± 0.9034i	- 0.0047 ± 0.0034i

**Table 2** (continued)

GA-UPFC-RFB [studied]	MFO-UPFC-RFB [proposed]
- 4.4049 ± 0.3975i	- 0.0065
- 5.8776 ± 0.0179i	- 0.0025 ± 0.0028i
- 0.5638 ± 2.1028i	- 0.0054
- 3.9242 ± 0.0888i	- 0.0039
- 0.4243 ± 1.6245i	- 0.0032
- 3.1503	- 0.0059
- 3.3996 ± 0.1595i	- 0.0059
- 3.4914	- 0.0037
- 5.8918	- 0.0024
- 3.3714 ± 0.0069i	- 0.0036
- 5.8921	- 0.0036
- 0.8667 ± 1.3313i	- 0.0036
- 0.5576 ± 1.4381i	- 0.0036
- 5.8923	- 0.0059
- 5.8923	- 0.0059
- 5.8923	- 0.0059
- 1.0152	- 0.0059
- 0.9299	- 0.0008 ± 0.0014i
- 0.8433	- 0.0013 ± 0.0011i
- 0.8136	- 0.0005 ± 0.0012i
- 0.8267	- 0.0004 ± 0.0011i
- 0.8265	- 0.0008 ± 0.0004i
- 0.6060	- 0.0010 ± 0.0000i
- 0.1511 ± 0.1097i	- 0.0005 ± 0.0003i
- 0.1123 ± 0.0918i	- 0.0008 ± 0.0001i
- 0.0908 ± 0.1017i	- 0.0007
- 0.0883 ± 0.0596i	- 0.0009
- 0.0659 ± 0.0556i	- 0.0002 ± 0.0001i
- 0.0972	- 0.0002 ± 0.0001i
- 0.0370	- 0.0002 ± 0.0000i
- 0.1153	- 0.0001
- 0.1161	- 0.0001
- 0.1160 ± 0.0000i	- 0.0001
- 0.0236	- 0.0001
- 0.1158	- 0.0001 ± 0.0000i
- 0.1158	- 0.0001
- 0.0054 ± 0.0091i	- 0.0001
- 0.0054 - 0.0091i	
- 0.0059 ± 0.0096i	
- 0.0057 ± 0.0096i	
- 0.0058 ± 0.0096i	
- 0.0058 ± 0.0096i	
- 0.0058 ± 0.0096i	

**Table 3** Comparative FOD and studied performance indices for the investigated controller types

Technique/controller type	FOD	Performance indices		
	ITAE	IAE	ITSE	ISE
GA-UPFC-RFB [studied]	7.1496	0.4001	0.0096	0.0009
MFO-UPFC-RFB [proposed]	<b>1.1706</b>	<b>0.1155</b>	<b>0.0022</b>	<b>0.0003</b>

designed controller minimizes the effects of load perturbation, as exist during the simulation time.

### 5.3 Scenario (c): Simultaneous application of random SLP in both area 1 and area 2

This case is presumed to be an even more difficult case as the same load (considered in scenario (b)) is simultaneously applied to area 1 and area 2. Corresponding to this, response plots are shown in Fig. 17. From Fig. 17, it may be observed that the same inferences may be drawn as studied in scenario (b). Thus, for the random load pattern, as applied to two different areas, the designed controller is still very effective in eliminating large oscillation.

**Table 4** Comparative transient details offered by different investigated controller types

Response profiles	GA–UPFC–RFB [studied]				MFO–UPFC–RFB [proposed]			
	$T_r$ (s)	$T_s$ (s)	$M_p$ (%)	$T_p$ (s)	$T_r$ (s)	$T_s$ (s)	$M_p$ (%)	$T_p$ (s)
$\Delta f_1$	$9.00 \times 10^{-4}$	33.16	0.120	5.3794	<b><math>6.28 \times 10^{-6}</math></b>	<b>26.96</b>	<b>0.0083</b>	<b>5.3744</b>
$\Delta f_2$	$2.17 \times 10^{-4}$	41.78	0.0077	5.53	<b><math>1.18 \times 10^{-4}</math></b>	<b>28.06</b>	<b>0.0050</b>	<b>5.9982</b>
$\Delta P_{tie12}$	0.0420	63.3109	0.0066	5.3475	<b><math>4.35 \times 10^{-4}</math></b>	<b>28.9889</b>	<b>0.0037</b>	<b>5.9805</b>
$\Delta P_{tie23}$	0.0071	62.5033	0.0015	17.3324	<b><math>6.17 \times 10^{-5}</math></b>	<b>27.75</b>	<b><math>6.71 \times 10^{-4}</math></b>	<b>7.49</b>
$ACE_1$	0.0127	57.185	0.0133	5.4262	<b>0.0015</b>	<b>28.4207</b>	<b>0.0081</b>	<b>5.7649</b>

**Table 5** System damping characteristics subjected to MFO–UPFC–RFB controller considering various uncertainty scenarios

Uncertainty	Case	% change	Signal	$M_p$ (%)	$T_p$ (s)	$T_s$ (s)	
Loading condition	Case 1	+ 25	$\Delta f_1$	0.0104	5.3672	30.27	
			$\Delta f_2$	0.0062	6.00	23.67	
			$\Delta P_{tie}$	0.004	5.98	32.35	
	Case 2	– 25	$\Delta f_1$	0.006	5.36	22.85	
			$\Delta f_2$	0.003	5.99	24.66	
			$\Delta P_{tie}$	0.0027	5.97	24.95	
	$T_g$	Case 3	+ 25	$\Delta f_1$	0.0083	5.37	27.39
				$\Delta f_2$	0.005	6.00	29.18
				$\Delta P_{tie}$	0.0037	5.98	29.18
Case 4	– 25	$\Delta f_1$	0.0083	5.37	27.15		
		$\Delta f_2$	0.005	6.00	24.08		
		$\Delta P_{tie}$	0.003	5.98	29.08		
$T_i$	Case 5	+ 25	$\Delta f_1$	0.0083	5.36	26.75	
			$\Delta f_2$	0.05	6.00	28.26	
			$\Delta P_{tie}$	0.0037	5.98	28.80	
	Case 6	– 25	$\Delta f_1$	0.008	5.36	27.12	
			$\Delta f_2$	0.005	5.98	28.49	
			$\Delta P_{tie}$	0.0037	5.98	29.09	

**Fig. 14** Comparative frequency deviation profiles offered by investigated damping controllers subjected to random SLP applied to area 1: **a**  $\Delta f_1$ , **b**  $\Delta f_2$ , **c**  $\Delta f_3$ , **d**  $\Delta f_4$ , **e**  $\Delta f_5$  and **f**  $\Delta f_6$

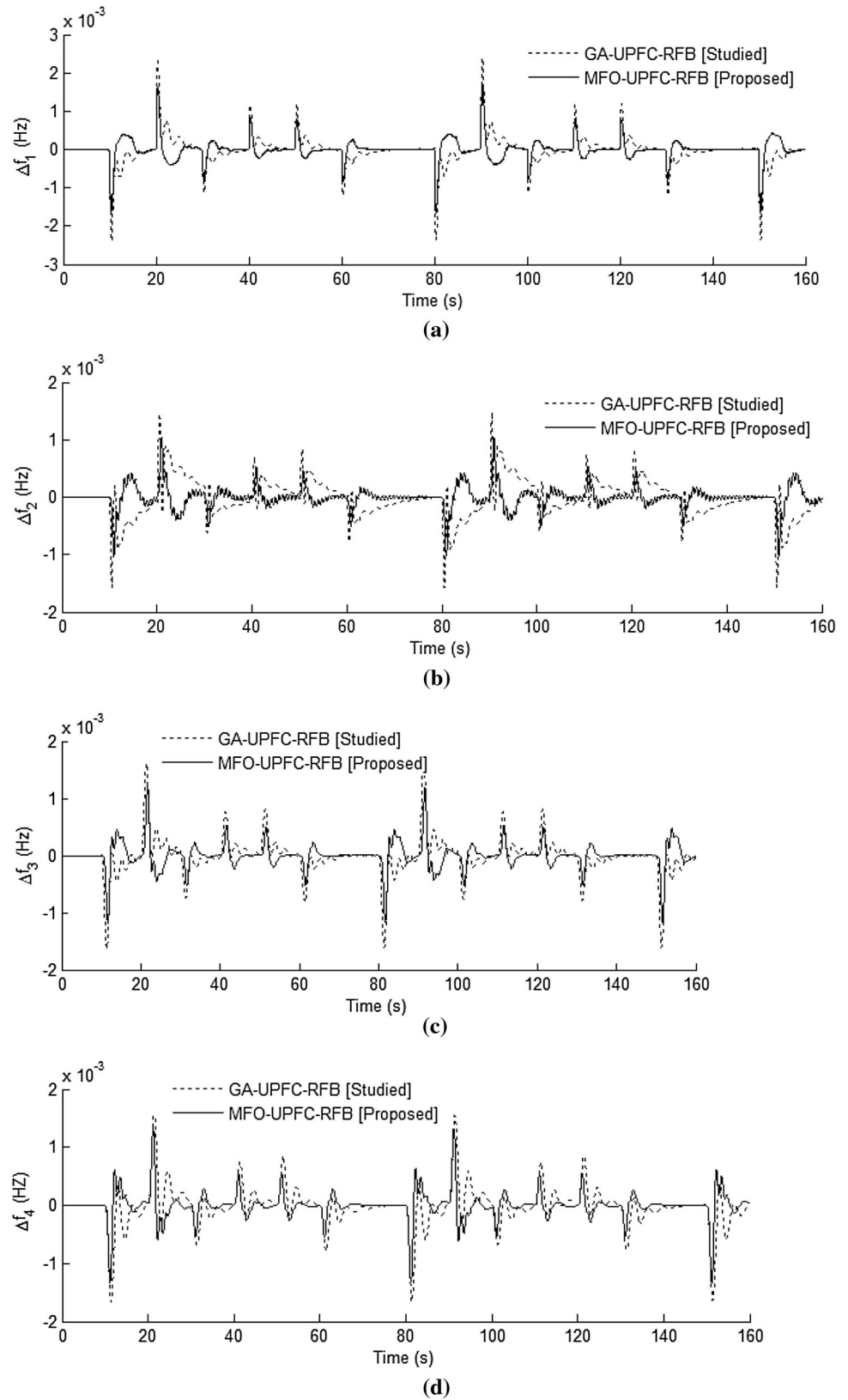
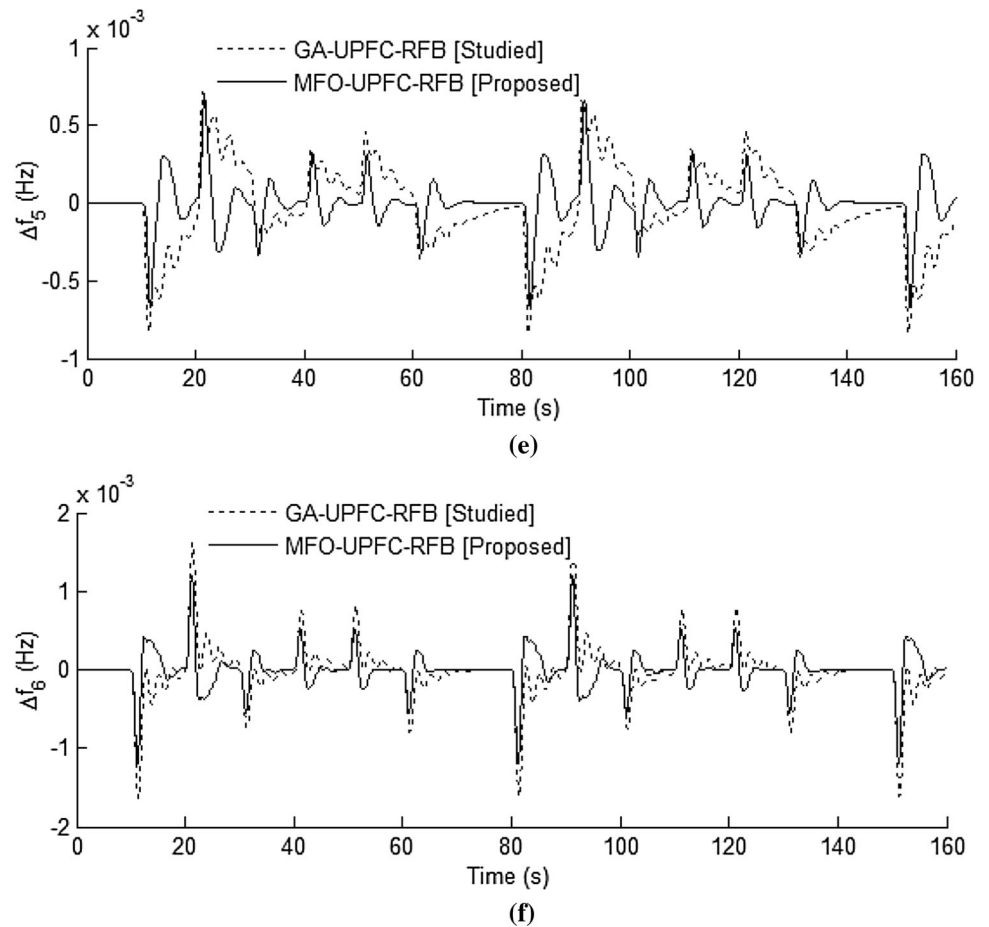


Fig. 14 continued



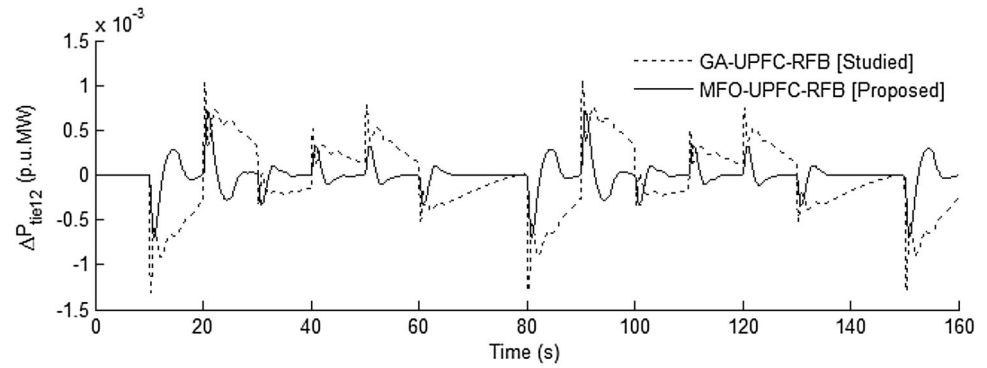
#### 5.4 Scenario (d): Sensitivity analysis of the proposed MFO–UPFC–RFB controller

In order to investigate the robustness of the proposed MFO–UPFC–RFB controller against wide variation in loading condition and other model parametric uncertainties, sensitivity analysis is performed. In the present work, sensitivity analysis is carried out by considering  $\pm 25\%$  uncertainties from their nominal ones in loading condition and in the values of  $T_g$ ,  $T_t$ ,  $T_{th}$  and  $T_w$ . The dynamic response plot of frequency deviation of area 1 with the parametric uncertainties is depicted in Fig. 18. While comparing Figs. 11, 12, 13, 14, 15, 16, 17, 18, it may be inferred that these two plots (i.e., of  $\Delta f_1$ ) are almost the same with the change in uncertainties considered. This study confirms that the proposed controller is quite robust under the circumstances of varying physical constraints.

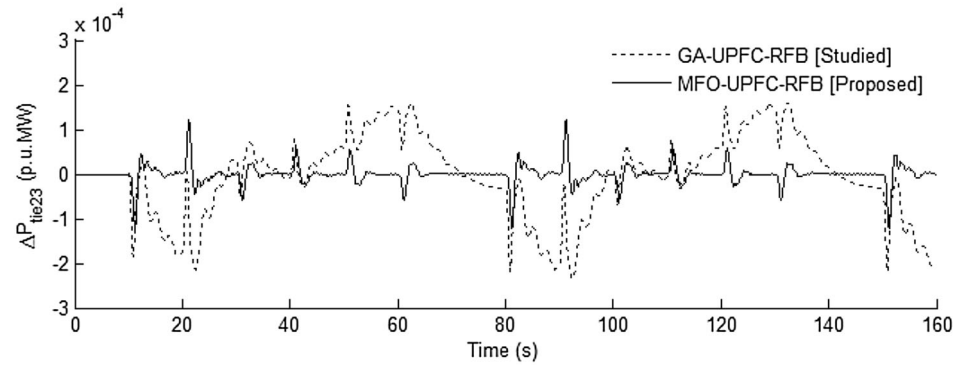
## 6 Conclusion

In this article, a more complete model, i.e., an interconnected six-area power system with diverse source of power generation imposing the effects of  $T_d$ , GDB, BD, reheat turbine and GRC has been satisfactorily, studied in reference to AGC prospective. The influences of UPFC, as well as RFB, as load frequency stabilization, have been studied and established. The primary contribution of the current article is the implementation of MFO algorithm in designing of the gains of the PID controller and the tuneable parameters of UPFC and RFB for improving the damping of oscillations. The simulation results reveal that the proposed MFO is a perfect fit for the parameter optimization problem and provides a better solution in comparison to other similar types of metaheuristic optimization techniques like GA. The frequency and tie-line power

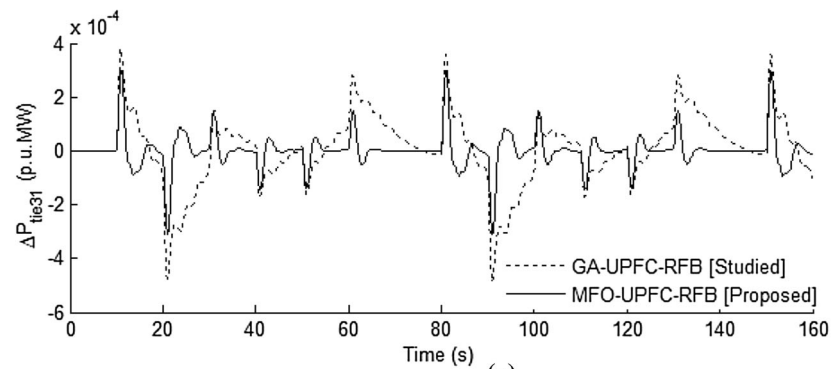
**Fig. 15** Comparative tie-line power deviation profiles offered by investigated damping controllers subjected to random SLP applied to area 1: **a**  $\Delta P_{tie12}$ , **b**  $\Delta P_{tie23}$ , **c**  $\Delta P_{tie31}$ , **d**  $\Delta P_{tie41}$ , **e**  $\Delta P_{tie52}$  and **f**  $\Delta P_{tie63}$



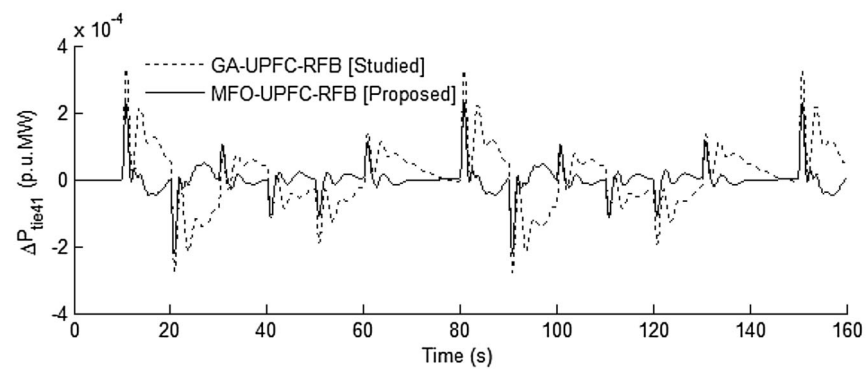
(a)



(b)



(c)



(d)

Fig. 15 continued

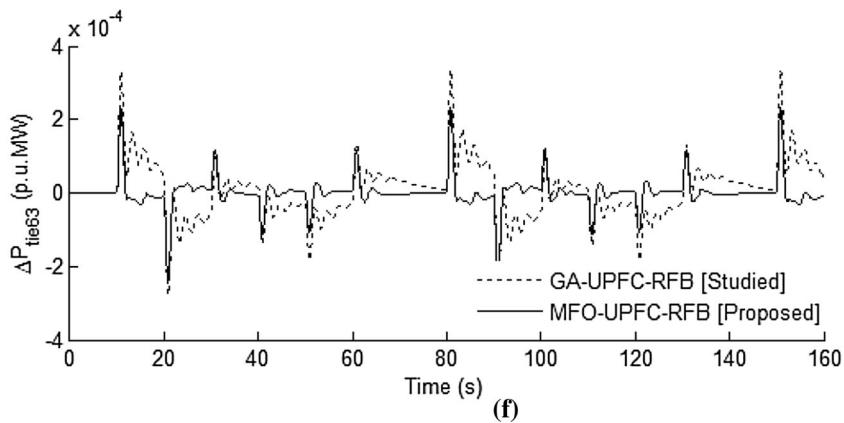
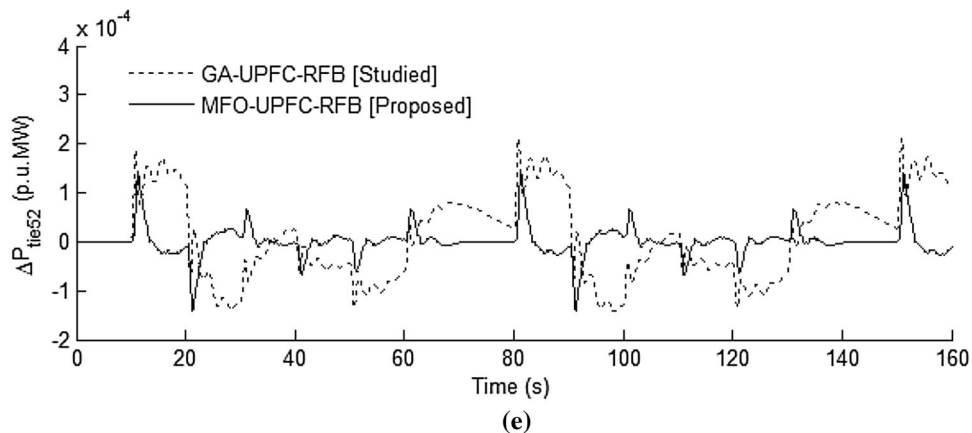
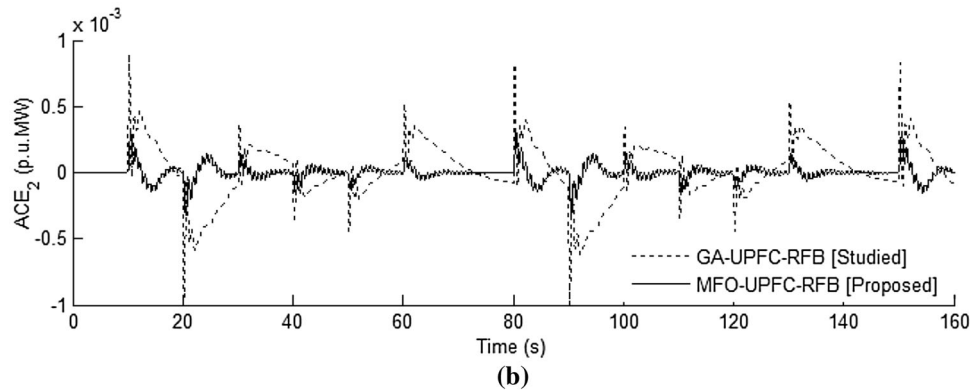
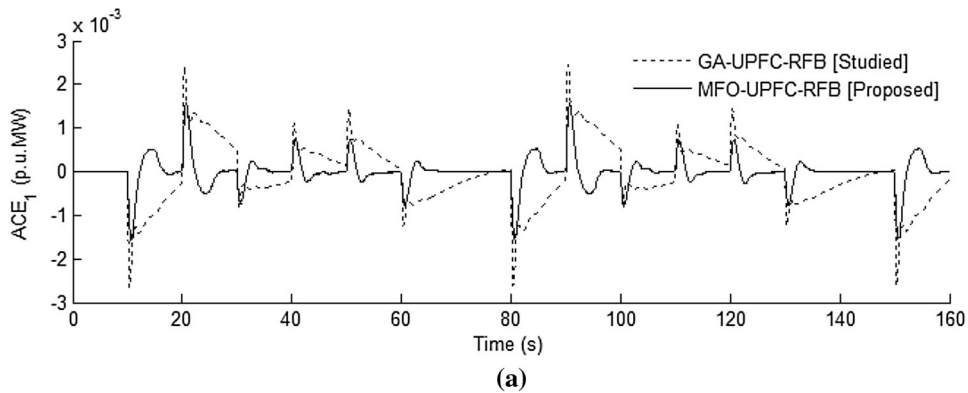
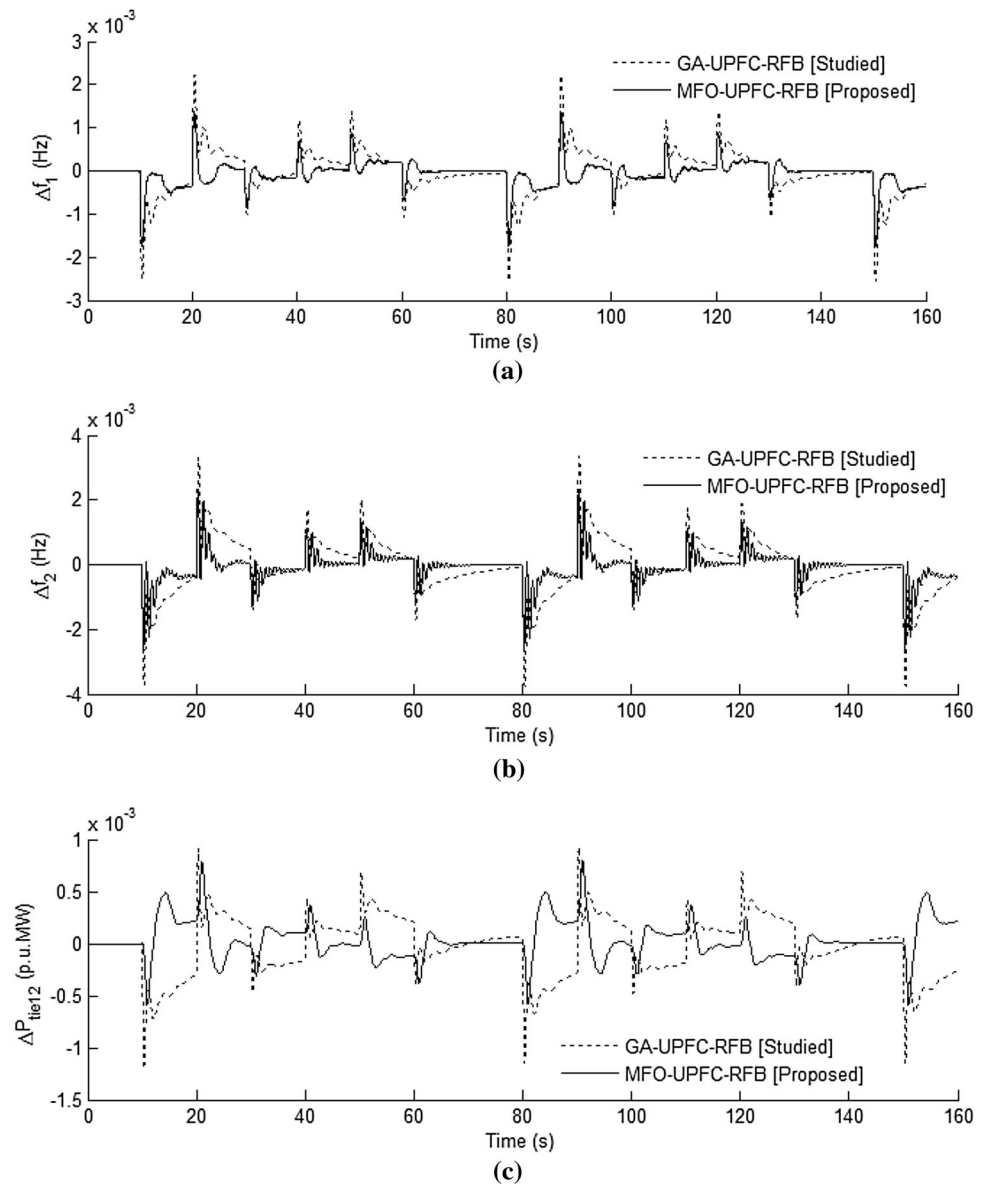


Fig. 16 Comparative dynamic response profiles of error signals of area 1 and area 2 offered by investigated damping controllers subjected to random SLP applied to area 1: **a**  $ACE_1$  and **b**  $ACE_2$



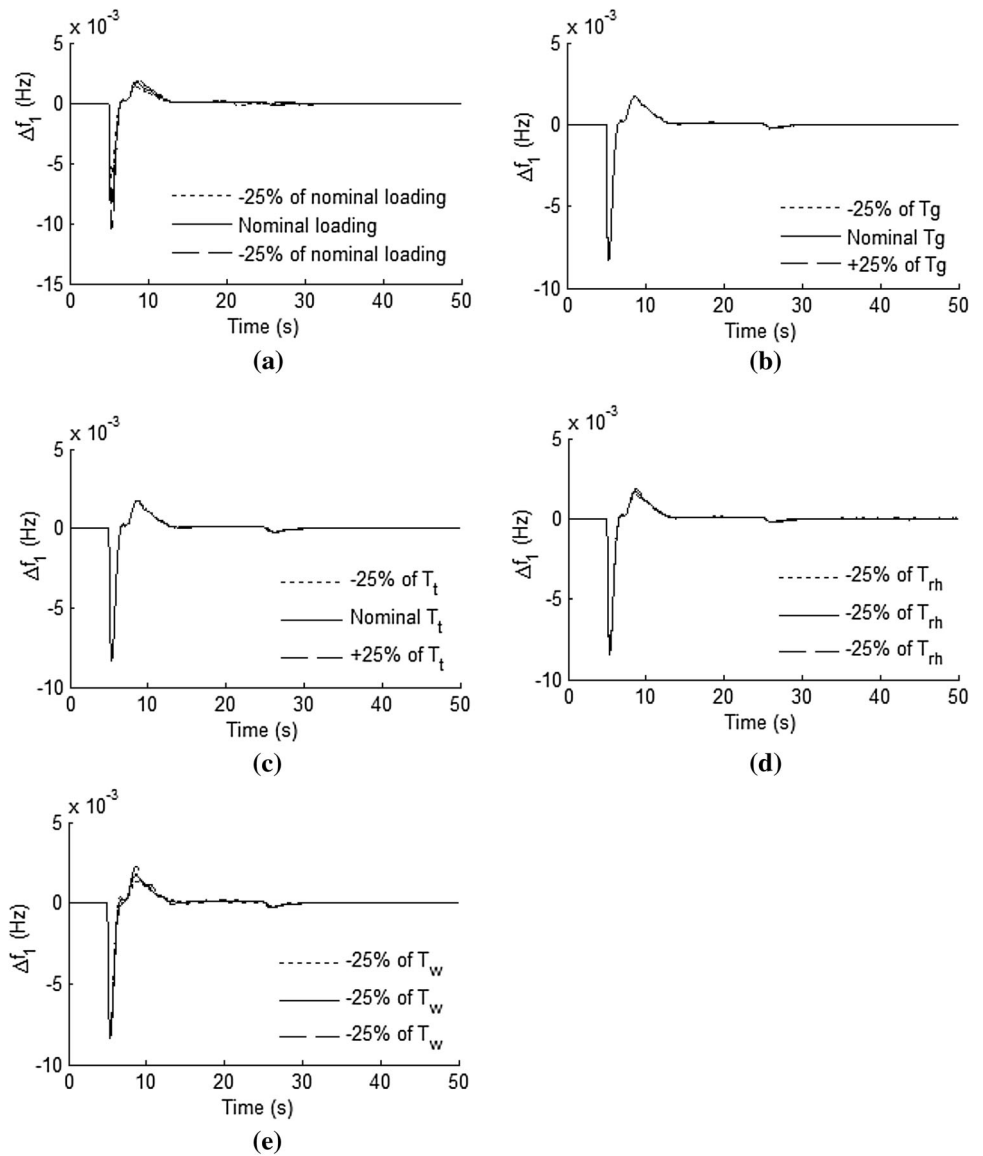
**Fig. 17** Comparative dynamic response profiles offered by investigated damping controllers subjected to simultaneous application of random SLP to both area 1 and area 2: **a**  $\Delta f_1$ , **b**  $\Delta f_2$  and **c**  $\Delta P_{tie12}$ .



deviation profile in individual areas have also been improved. As viewing performance indices, the system performance using MFO-based MFO-UPFC-RFB controller is justified. The sensitivity analysis of the present

work also verifies this. Therefore, the illustrated work may be quite useful in some realistic sense for practical power system in the context of AGC perspective while employing MFO as an optimizing tool.

**Fig. 18** Frequency deviation profile of area 1 ( $\Delta f_1$ ) using the proposed MFO–UPFC–RFB controller with  $\pm 25\%$  deviation in: **a** rated loading, **b**  $T_g$ , **c**  $T_t$ , **d**  $T_{rh}$  and **e**  $T_w$



## Appendix

### Nominal Data of the Designed Six-Area Power System Model (Sahu et al. 2014)

System configuration  $f = 60$  Hz,  $P_{r1} = P_{r2} = P_{r3} = P_{r4} = P_{r5} = P_{r6} = 2000$  MW, Total area load = 1840 MW, base rating = 2000 MW, initial loading = 92%

For reheat turbine unit  $a_{ij} = -1$ ,  $B_i = 0.4312$  p.u.MW/Hz,  $K_{ri} = 0.3$ ,  $K_{pi} = 68.9655$  Hz/p.u.MW,  $R_{ii} = 2.4$  Hz/p.u.MW,  $T_{ij} = 0.0433$ ,  $T_{gi} = 0.06$  s,  $T_{pi} = 11.49$  s,  $T_{ri} = 10.2$  s,  $T_{ii} = 0.3$  s

For hydro turbine unit  $T_{ghi} = 0.2$ ,  $R_h = 2.4$  Hz/p.u.MW,  $T_{thi} = 28.749$  s,  $T_{tsi} = 4.9$  s,  $T_{wsi} = 1.1$  s

For gas turbine unit  $b_g = 0.049$  s,  $c_g = 1$ ,  $R_g = 2.4$  Hz/p.u.MW,  $X_c = 0.6$  s,  $Y_c = 1.1$  s,  $T_{cd} = 0.2$  s,  $T_{cr} = 0.01$  s,  $T_f = 0.239$  s

Participation factors  $K_T = 0.543478$ ,  $K_H = 0.326084$ ,  $K_G = 0.130438$ .

### Imposed Nonlinearities

Physical constraints (Sahu et al. 2014, 2015) GRC = 3%/min for thermal unit whereas 270%/min for rising generation and 360%/min for lower generation for hydro unit,  $T_d = 50$  ms,  $N_1 = 0.8$ ,  $N_2 = \frac{-0.2}{\pi}$ .



Boiler dynamics  
(Chandrakala and  
Balamurugan 2016)

$$K_1 = 0.85, K_2 = 0.095, K_3 = 0.92,$$

$$C_B = 200, T_D = 0 \text{ s}, T_F = 10 \text{ s},$$

$$K_{IB} = 0.030, T_{IB} = 26 \text{ s},$$

$$T_{RB} = 69 \text{ s}$$

### Data for UPFC Controller

GA-based  $K_{upfc} = 0.2586, T_{upfc} = 0.0400\text{s}, T_w = 22.3831,$   
 $T_1 = 0.4498 \text{ s}, T_2 = 0.0673 \text{ s}, T_3 = 0.8829 \text{ s},$   
 $T_4 = 0.0439 \text{ s}$

MFO-  
based  $K_{upfc} = 0.5263, T_{upfc} = 0.0010\text{s}, T_w = 1.3931,$   
 $T_1 = 1.0 \text{ s}, T_2 = 0.6860 \text{ s}, T_3 = 0.0010 \text{ s},$   
 $T_4 = 0.1582 \text{ s}$

### Data for RFB Controller

GA-  
based  $K_{rfb1} = 0.5824, T_{rfb1} = 0.8244 \text{ s}, K_{rfb2} = 0.9571, T_{rfb2} =$   
 $0.1571 \text{ s} .$

MFO-  
based  $K_{rfb1} = 0.9742, T_{rfb1} = 0.0010 \text{ s}, K_{rfb2} = 0.9424, T_{rfb2} =$   
 $0.0895 \text{ s}$

## References

- Abdel-Magid YL, Dawoud MM (1995) Genetic algorithms applications in load frequency control genetic algorithms in engineering systems: innovations and applications. Presented at the first international conference on (Conf. Publ. No. 414), GALESIA
- Arya Y (2018) Automatic generation control of two-area electrical power systems via optimal fuzzy classical controller. *J Frankl Inst* 355:2662–2688
- Bevrani H (2009) Intelligent automatic generation control. Springer, New York
- Bhatt P, Ghoshal SP, Roy R (2012) Coordinated control of TCPS and SMES for frequency regulation of interconnected restructured power systems with dynamic participation from DFIG based wind farm. *Renew Energy* 40:40–50
- Chandrakala KRMV, Balamurugan S (2016) Simulated annealing based optimal frequency and terminal voltage control of multi-source multi area system. *Int J Electr Power Energy Syst* 78:823–829
- Chidambaram IA, Paramasivam B (2013) Optimized load-frequency simulation in restructured power system with redox flow batteries and interline power flow controller. *Int J Electr Power Energy Syst* 50:9–24
- Das S, Abraham A, Konar A (2008) Particle swarm optimization and differential evolution algorithms: technical analysis, applications and hybridization perspectives. *Adv Comput Intell Ind Syst* 116:1–38
- Debbarma S, Saikia LC, Sinha N (2014) Automatic generation control using two degree of freedom fractional order PID controller. *Int J Electr Power Energy Syst* 58:120–129
- Enomoto K, Sasaki T, Shigematsu T, Deguchi H (2002) Evaluation study about redox flow battery response and its modeling. *IEEJ Trans Power Eng* 554:122–160
- Golpira H, Bevrani H, Golpira H (2011) Application of GA optimization for automatic generation control design in an interconnected power system. *Energy Convers Manag* 52:2247–2255
- Gorripotu TS, Sahu RK, Panda S (2015) AGC of a multi-area power system under deregulated environment using redox flow batteries and interline power flow controller. *Eng Sci Technol* 18:555–578
- Gozde H, Cengiz Taplamacioglu M, Kocaarslan I (2012) Comparative performance analysis of Artificial Bee Colony algorithm in automatic generation control for interconnected reheat thermal power system. *Int J Electr Power Energy Syst* 42:167–178
- Guha D, Roy PK, Banerjee S (2016) Load frequency control of interconnected power system using grey wolf optimization. *Swarm Evol Comput* 27:97–115
- Guha D, Roy PK, Banerjee S (2018) Application of backtracking search algorithm in load frequency control of multi-area interconnected power system. *Ain Shams Eng J* 9:257–276
- Kouba NEIY, Mena M, Hasni M, Boudour M (2016) LFC enhancement concerning large wind power integration using new optimized PID controller and RFBs. *IET Gener Transm Distrib* 10:4065–4077
- Mirjalili S (2015) Moth-flame optimization algorithm: a novel nature-inspired heuristic paradigm. *Knowl Syst* 89:228–249
- Mondal D, Chakrobarat A, Sengupta A (2014) Power system, small signals stability and control, 1st edn. Academic Press, Cambridge, pp 76–82
- Nise NS (2006) Pomana: control system engineering, 6th edn. Wiley, New York
- Ogata K (1995) Modern control engineering, 2nd edn. Printice Hall International, Upper Saddle River
- Panda S, Swain SC, Mahapatra S (2015) A hybrid BFOA–MOL approach for FACTS-based damping controller design using modified local input signal. *Int J Electr Power Energy Syst* 67:238–251
- Parmar KPS, Majhi S, Kothari DP (2012) Load frequency control of a realistic power system with multi-source power generation. *Int J Electr Power Energy Syst* 42:426–433
- Pedersen MEH, Chipperfield AJ (2010) Simplifying particle swarm optimization. *Appl Soft Comput* 10:618–628
- Pradhan PC, Sahu RK, Panda S (2016) Firefly algorithm optimized fuzzy PID controller for AGC of multi-area multi-source power systems with UPFC and SMES. *Eng Sci Technol* 19(1):338–354
- Raju M, Saikia LC, Sinha N (2016) Automatic generation control of a multi-area system using ant lion optimizer algorithm based PID plus second order derivative controller. *Int J Electr Power Energy Syst* 80:52–63
- Sahu RK, Panda S, Yegireddy NK (2014) A novel hybrid DEPS optimized fuzzy PI/PID controller for load frequency control of multi-area interconnected power systems. *J Process Control* 24:1596–1600
- Sahu BK, Patia S, Mohanty PK, Panda S (2015a) Teaching-learning based optimization algorithm based fuzzy-PID controller for automatic generation control of multi-area power system. *Appl Soft Comput* 27:240–249
- Sahu RK, Panda S, Padhan S (2015b) A hybrid firefly algorithm and pattern search technique for automatic generation control of multi area power systems. *Int J Electr Power Energy Syst* 64:9–23
- Sahu RK, Panda S, Padhan S (2015c) A novel hybrid gravitational search and pattern search algorithm for load frequency control of nonlinear power system. *Appl Soft Comput* 29:310–327
- Sahu RK, Sekhar GTC, Panda S (2015d) DE optimized fuzzy PID controller with derivative filter for LFC of multi-source power system in deregulated environment. *Ain Shams Eng J* 6:511–530

- Sahu RK, Gorripotu TS, Panda S (2015e) A hybrid DE-PS algorithm for load frequency control under deregulated power system with UPFC and RFB. *Ain Shams Eng J* 6:893–911
- Saikia LC, Sahu SK (2013) Automatic generation control of a combined cycle gas turbine plant with classical controllers using firefly algorithm. *Int J Electr Power Energy Syst* 53:27–33
- Saikia LC, Nanda J, Mishra S (2011) Performance comparison of several classical controllers in AGC for multi-area interconnected thermal system. *Int J Electr Power Energy Syst* 33:394–401
- Shabani H, Vahidi B, Ebrahimpour M (2013) A robust PID controller based on imperialist competitive algorithm for load-frequency control of power systems. *ISA Trans* 52:88–95
- Shiva CK, Mukherjee V (2016) Design and analysis of multi-source multi-area deregulated power system for automatic generation control using quasi-oppositional harmony search algorithm. *Int J Electr Power Energy Syst* 80:382–395
- Verma KS, Singh SN, Gupta HO (2001) Location of unified power flow controller for congestion management. *Electr Power Syst Res* 58:89–96
- Zare K, Hagh MT, Morsali J (2015) Effective oscillation damping of an interconnected multi-source power system with automatic generation control and TCSC. *Int J Electr Power Energy Syst* 65:220–230